3-11-2011

Changes to Electrical Conductivity in Irradiated Carbon Nanocomposites

Nickolas A. Duncan

CHANGES TO ELECTRICAL CONDUCTIVITY IN IRRADIATED CARBON NANOCOMPOSITES

THESIS

Nickolas A. Duncan, Captain, USA

AFIT/GNE/ENP/11-M06

DEPARTMENT OF THE AIR FORCE
AIR UNIVERSITY

AIR FORCE INSTITUTE OF TECHNOLOGY

Wright-Patterson Air Force Base, Ohio

AFIT/GNE/ENP/11-M06

CHANGES TO ELECTRICAL CONDUCTIVITY IN IRRADIATED CARBON NANOCOMPOSITES

THESIS

Presented to the Faculty

Department of Engineering Physics

Graduate School of Engineering and Management

Air Force Institute of Technology

Air University

Air Education and Training Command

In Partial Fulfillment of the Requirements for the

Degree of Master of Science in Nuclear Engineering

Nickolas A. Duncan, BS

Captain, USA

March 2011

AFIT/GNE/ENP/11-M06

CHANGES TO ELECTRICAL CONDUCTIVITY IN IRRADIATED CARBON NANOCOMPOSITES

Nickolas A. Duncan, BS

Captain, USA

Approved:

LTC John W. McClory, (Chairman)	01 March 2011 Date
Shanker Mall, PhD (Member)	01 March 2011 Date
James Petrosky, PhD (Member)	01 Mar 11 Date

Abstract

Carbon nanotubes (CNT) and carbon nanofibers (CNF) are two nanoparticles incorporated in a polymer to create a composite material. These composites are two potential lightweight materials for use as replacements for aluminum structures on satellite systems. Both composite materials have the low resistivity that is consistent with conductive materials. However, the CNT composite is substantially more conductive than the CNF composite. The CNT and CNF composites were irradiated with electrons and neutrons to fluence levels of $1\times10^{16} e^{-}/cm^{2}$ and $1.11\times10^{14} neutrons/cm^{2}$. No changes were observed in the resistivity of the CNF composites following neutron and electron irradiation. A 3.7% increase in resistivity was observed for the CNT composite following neutron irradiation and a 25.5% increase in resistivity following electron irradiation. An additional electron irradiation was conducted on both composites to a fluence of $6\times10^{16} e^{-}/cm^{2}$. Again, no change in resistivity was observed in the CNF composites, while an 8.1% increase in resistivity was observed in the CNT composite. In addition, the CNT composite resistivity recovered after 240 hours while at room temperature. A neutron irradiation was conducted on both composites to a fluence of $4\times10^{16} neutrons/cm^{2}$. No change in the resistivity was observed in the CNF composite, while a steady increase in resistivity was observed in the CNT composites as a function of neutron dose.

Table of Contents

Page

List of Figures

Figure Page

Figure Page

List of Tables

Table Page

List of Symbols and Acronyms

Å	Angstrom [10^{-10} meters]
A	Ampere measure of current
AFIT	Air Force Institute of Technology
ASTM	American Society for Testing and Materials
CNF	Carbon NanoFiber
CNT	Carbon NanoTube
CASINO®	Monte Carlo Simulation of Electron Trajectories in Solids
CPT	Captain, US Army
cm	Centimeter [.01 meters]
σ	Conductivity
DMM	Digital Multimeter
eV	Electron Volt
EMI	Electromagnetic Interference
ESD	Electrostatic Discharge
ESR	Electron Spin Resonance
GEO	Geosynchronous Earth Orbit
gsm	Grams per square meter [references nanofiller content]
HDPE	High Density Polyethylene
I	Current [A]
IV	Current verses Voltage
keV	Kilo Electron Volt [10^3 eV]
kV	Kilo Volt [10^3 V]

mA	Milliamp [10^{-3} A]
mΩ	Milliohm [10^{-3} Ohm]
MAJ	Major, U.S. Army
MeV	Mega Electron Volt [10^{6} eV]
MIL-STD	Military Standard
µm	Micrometer [10^{-6} meter]
MWNT	Multi Walled NanoTube
nA	Nanoamp [10^{-9} A]
NASA	National Aeronautics and Space Administration
Ni	Nickel
NiOH	Nickel Hydroxide
NiO	Nickel Oxide
NIST	National Institute of Standards and Technology
OSURR	The Ohio State University Research Reactor
torr	Measure of Pressure (vacuum) torr = 133.3 Pa
Ω	Resistance [Ω]
ρ	Resistivity [Ω-cm]
rad	Radiation Absorbed Dose
RT	Room Temperature
sec	Second
SWNT	Single Walled NanoTube

CHANGES TO ELECTRICAL CONDUCTIVITY IN IRRADIATED CARBON NANOCOMPOSITES

I. Introduction

1.1 Background

Advanced composite materials have been investigated to reduce the cost and increase the functionality of space systems. The satellite bus, historically made from aluminum, is under consideration for incorporation of advanced composites. Aluminum, a conducting metal, has the appropriate strength and conductive properties to protect the internal components of a satellite system. The disadvantage of aluminum is its weight. Therefore, lightweight reinforced carbon composites have been identified to replace the aluminum bus. The fiber composites and polymers meet the thermal and mechanical requirements for space use, but do not necessarily meet the requirements of protection from electromagnetic and high energy radiation effects. By incorporating conductive nanofiller material into the composites and adhesives, the mechanical, thermal, and electrical properties are enhanced. The nanofillers decrease the resistive properties of the composite sufficient to meet electromagnetic design requirements while maintaining the substantial weight savings over aluminum.

Over time, dielectric materials potentially build up large charge differentials in the space environment. If there is no mechanism for relaxing the material back to charge equilibrium, the potential difference eventually supersedes the material's ability to

contain the charge and the material breaks down. When the material breaks down, it releases its charge through an electrostatic discharge (ESD). ESD is a parasitic phenomena experienced by all materials in space to varying degrees of destructiveness; from routine charge relaxation to high current arcing resulting in component burn-out or total vehicle failure [1].

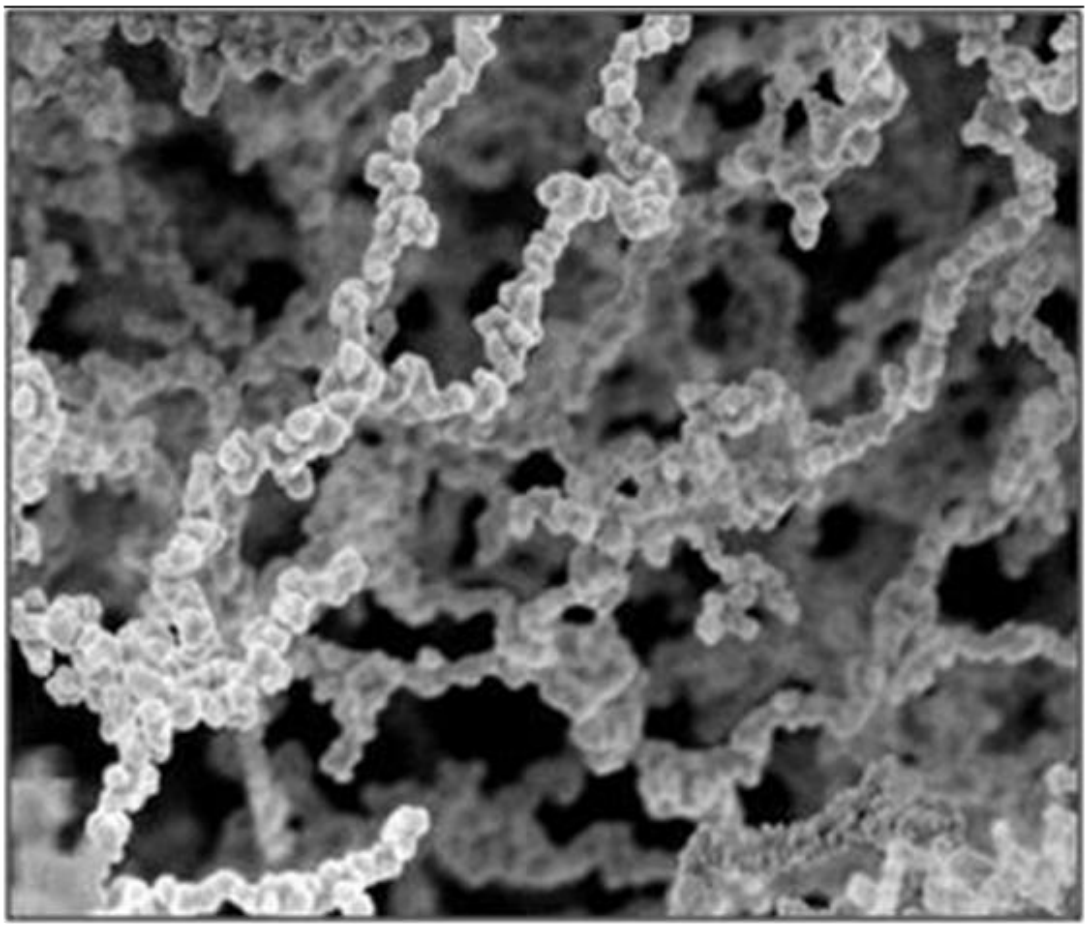

Figure 1. Nickel Nanostrands approximately 100 nm in diameter [4].

Previous to this work, composite nanofillers with nickel nanostrands were investigated in a similar fashion as this work. [1] [2] An image of a nickel nanostrand is

depicted in Figure 1. The resistivity and electrostatic properties of the nickel nanostrand, both pre and post electron irradiation, are characterized in that research and used to validate and compare the results in this research effort.

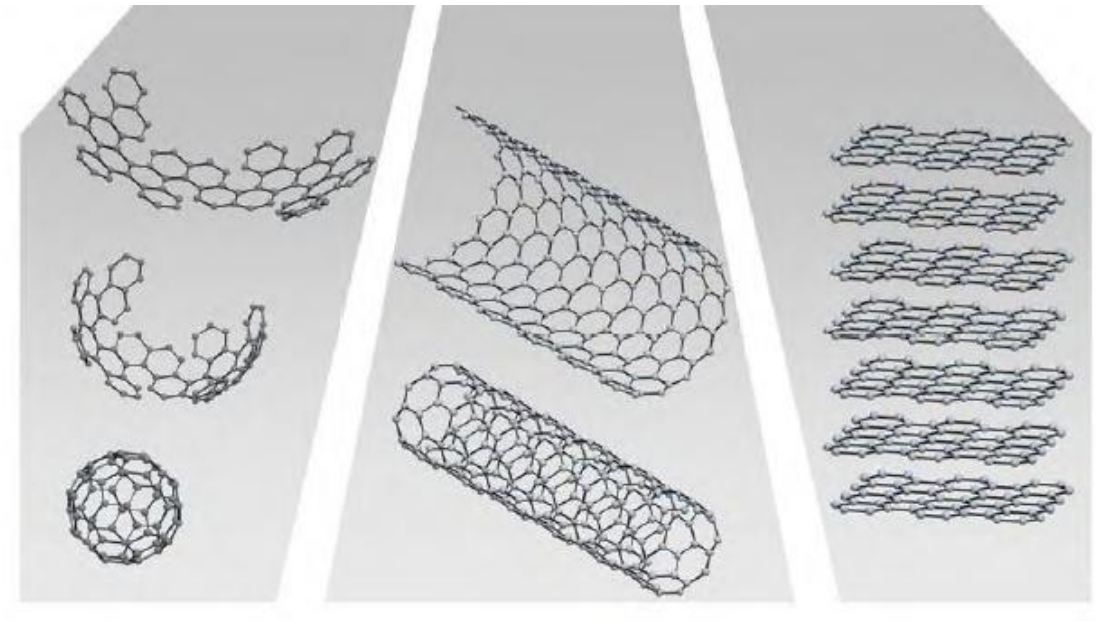

Figure 2. Depiction of a Carbon Nanotube created by rolling a two dimensional graphene sheet into a tube (center) the graphene sheets have also been rolled into balls (left) or stacked on top of each other (right). [5]

Carbon nanotubes (CNT) have been introduced into space grade composites as a method of increasing conductivity. A depiction of a single walled nanotube (SWNT) CNT is shown in Figure 2. The CNTs are electrically conductive and have the capability to discharge electrostatic potentials. They also provide sufficient conductivity and even shield from the radio frequency interference, while keeping a high strength-to-weight ratio. Since the discovery of the CNT and their high strength and conductive properties, a large amount of research in many fields has gone into the study of CNT's. Potential

applications of CNT's include energy storage devices, field emission devices, transistors, sensors and probes [3]. Little research has been conducted on the ionizing and non-ionizing radiation effects of CNT's in composites. The high cost of CNT composite fabrication may prevent the use as opposed to other materials.

Carbon nanofibers (CNF) have been introduced into space grade composites as a method of increasing conductivity. A TEM image of a CNF is shown in Figure 3. CNF's are electrically conductive and have the capability to discharge large electrostatic potentials. The CNF is similar to a CNT except the outer wall is not one atom thick like a CNT. The CNF can be thought of as stacked layers of graphene in tube-like structures. This makes CNF's larger in diameter than CNT's, but they have similar mechanical and electrical properties.

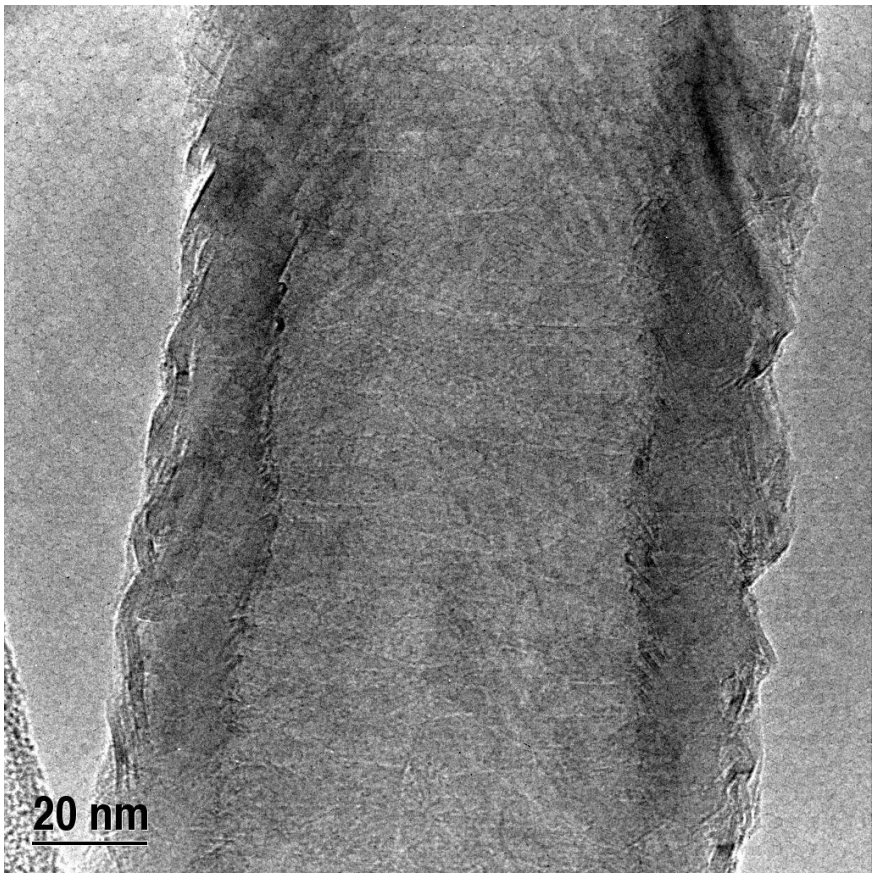

Figure 3. A transmission electron microscope (TEM) image of PR-25-XT-HHT carbon nanofiber shows the highly graphitic structure of the nanomaterial. [6]

A generic CNT outside of a polymer is more conductive than a CNF. The CNT conductivity is on the same order of magnitude as a conductive piece of metal such as nickel. The CNF outside of a polymer is still considered a conductive material. The low manufacturing cost of the CNFs compared to CNTs makes them desirable as a nanofiller.

1.2 Objective

The objective of this work is to determine the effects of ionizing and non-ionizing radiation on resistivity and electrostatic discharge of these composite materials. The primary purpose is to determine the effects of a simulated space environment on

composite materials to include both the radiation and thermal environmental conditions. Furthermore, since previously reported volume resistivity changes following irradiation on the nickel nanostrand composites have been inconsistent, this thesis will also focus on improving the experimental procedures to obtain consistent results.

The primary objectives of this work are:

1. Establish a experimental capability to measure resistivity through fabricating platforms and developing procedures to produce consistent measurement results. The results can be used to validate previous research and follow-on experiments.

2. Measure and compare the resistivity of carbon nanotube and carbon nanofiber composites before and after electron and neutron irradiation.

3. Measure the ESD properties of both carbon nanofiber and carbon nanotube composite materials before and after irradiations for comparison.

4. Determine which nanofiller composite is less susceptible to space radiation damage.

A secondary objective of this work is to measure and compare the resistivity of nickel nanostrand, carbon nanotube , and carbon nanofiber composites before and after thermal cycling.

The electrical properties of the CNT and CNF composites will make both composites suitable replacements for aluminum as satellite structures. The CNT composite will be more conductive than the CNF composite when the composite material is volume loaded to the same percent. Due to the single atomic layer of the CNT's, they will be more susceptible to radiation damage. The wall thickness associated with CNF's will increase the radiation hardness of the CNF composite.

The reduction in the conductivity of the CNT composite will be greater due to radiation induced atomic displacements in the CNT nanoparticles. This is contrary to the

proposed reason for nickel nanostrand radiation damage effects from previous research, where the increase in resistivity was believed to be largely due to interactions with the epoxy resin. This is due to the nanofiller in the CNT and CNF composites consisting of carbon, a natural semiconducting material, and it being more susceptible to radiation damage as opposed to nickel. Neutron radiation should have a larger impact on the resistivity due to its non-ionizing radiation effects compared to electron radiation.

1.3 Paper Organization

This thesis will address theory, experimental design, results and analysis, and provide conclusions and recommendations. The theory section will briefly describe the space environment and a description of the materials under investigation. The experiment section describes the design of the experiments, the measurements and procedures, and provides relevant explanations of specialized measurement techniques. Pre-irradiation and pre-thermal cycling measurements will also be presented in the experiment section. The results and analysis section presents results of the post-irradiation and post-thermal cycling measurements and analysis of those results. Finally, the conclusions and recommendations section offers analysis of the outcome from the experiment and recommendations for follow-on research.

II. Theory

2.1 Characterizing the Problem

2.1.1 The Space Environment

Space applications are of primary interest for the nanocomposites under investigation. Specifically, the thermal and radiation environments present in near-earth space will be defined in order to replicate them in experiments. The thermal and radiation effects on the nanocomposites will be investigated with respect to the surface and bulk resistivity changes. Satellites in geosynchronous orbit circle the earth approximately 35,000 km above the equator in the outer Van Allen radiation belt [7]. The radiation belts are characterized by energetic charged particles, primarily protons and electrons, which are trapped in regions above the earth by its magnetic field. An illustration of the Van Allen belts is provided in Figure 2. [8]

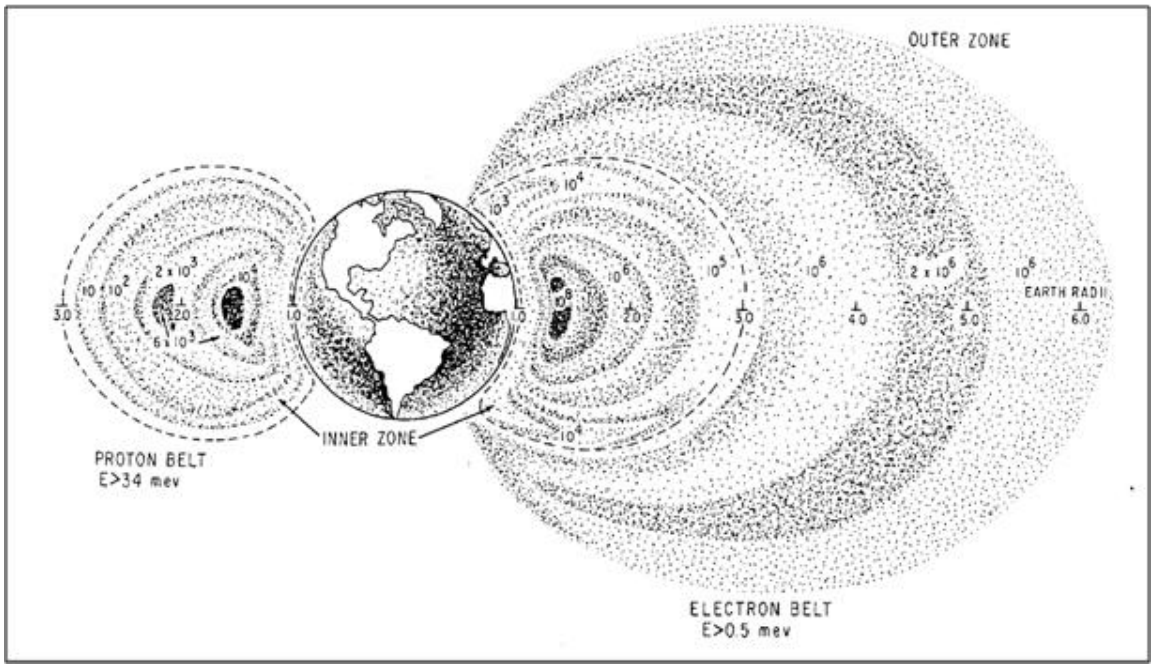

Figure 4. Schematic of the Earth's magnetosphere and associated plasma current densities [8]

Most satellites operate within a high energy particle buffer provided by the magnetosphere from 300 to1000 km. The magnetosphere effectively reduces the flux of high energy particles emanating from the solar wind by deflecting the particles away from the earth. Many of these particles are deflected into the tail current that extends thousands of Earth radii away from the earth. As these particles move through counter-current flow back into proximity with the earth, most particles are attenuated through collisions into a plasma, at an average energy range of 2 to 200 keV [2]. Under normal solar conditions, some high energy electrons remain in the plasma, with average energies of 100 keV to 100 MeV [7]. This effect is magnified during periods of high solar activity.

Of these high energy particles, electrons are of primary concern. The high energy electrons can cause damage to the internal components of a space vehicle. They generally do not contribute to surface charging effects as they penetrate the surface materials. As such, the lower energy electrons are primarily responsible for surface charging and the associated ESD [9]. For the purpose of space operation validation and evaluation, the space radiation environment is defined by MIL-STD-1809. MIL-STD-1809 defines flux values for proton and electron radiation at several altitudes.

Table 1. Energy flux values for protons and electrons defined by MIL-STD-1809 [10].

Source	Energy Range [MeV]	Flux [particles/cm^2-sec]
Protons	> 0.1	1×10^7
	> 1.0	1×10^3
Electrons	> 0.1	2×10^7
	> 0.5	8×10^6
	> 1.0	2×10^6
	> 2.0	2×10^4

The thermal space environment results in extreme temperature shifts in the satellite structural materials. An orbiting spacecraft repeatedly passes through day and night, referred to as a thermal cycle. A satellite in low-earth orbit (LEO) can be subjected to temperature differences from -80 to +80 ^{o}C [11]. Over the lifetime of a satellite, this equates to thousands of thermal cycles. Therefore, materials need to be able to maintain their electrical and mechanical properties under these extreme temperature shifts.

2.1.2 Nanocomposites

The three general types of nanocomposites under investigation are Nickel Nanostrands, Carbon Nanotube (CNT), and Carbon NanoFiber (CNF). In general, all three types use the same principle of incorporating a nanofiller in order to increase the conductivity of the composite. Figure 5 shows how a conductive nanoparticle such as CNT, CNF or nickel nanostrands can be incorporated into an insulating polymer to create a conductive material. The nanoparticles provide a conductive pathway through the polymer based composite. The conductivity is based upon the overall weight loading percent of the nanoparticle. Figure 6 shows how the resistivity decreases as a function of the volume percent of conductive nanoparticle, in this case nickel nanostrands, contained in the composite.

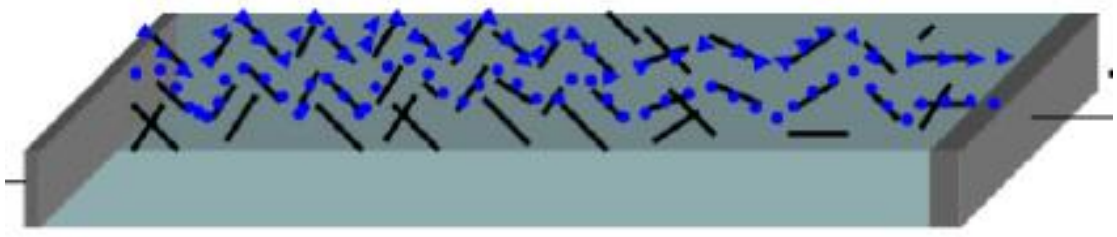

Figure 5. Concept of incorporating nanoparticles inside a polymer to create a conductive material. The nanofiller acts as a conductive pathway to increase the conductivity of the insulating polymer. [12]

Nickel nanostrand composite description and fabrication are described in [1] and [2] in great detail. As described by [1], the nickel nanostrand composites were fabricated with eight separate configurations. Only the control and external configurations were used in this thesis during the thermal cycle experiment. It is recommended to refer to [1] and [2] for more details concerning the nickel nanostrand composites.

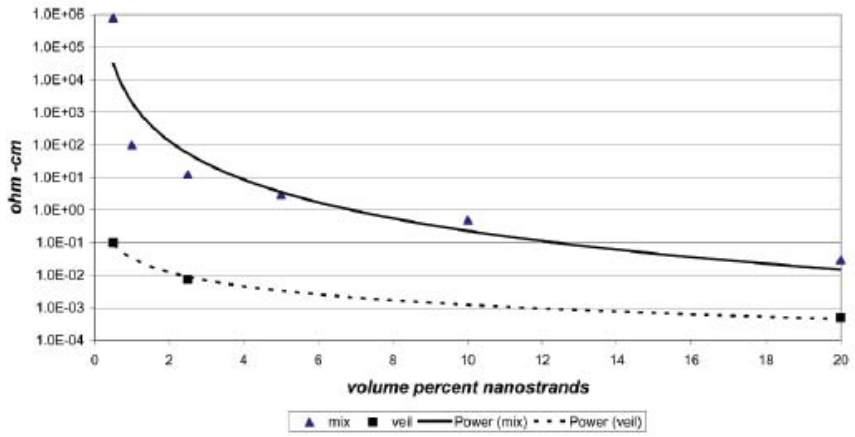

Figure 6. The decrease in resistivity as a function of volume percent of Nickel Nanostrands in a composite material [4]

The CNT composites were provided by Nanocomp, Inc. The actual CNT's are dispersed in 5250-4 epoxy resin on top of 6781 S-glass laminate substrate. The entire sample is 1 mm thick with the CNT and resin layer being a nominal 150 µm thick. The CNT's contained in the epoxy resin are estimated to be 25 nm in diameter and up to a millimeter in length [13]. The CNT samples consist of both multiwall and single wall nanotubes. The ratio of SWNT and MWNT contained in the composite is unknown. The CNT layer contains 20 $grams / m^2$ (gsm) of CNT's [13]. Figure 7 shows an SEM image of the CNT and CNF samples. As shown in Figure 7, the surface and the interface between the conductive layer and S-glass is not completely smooth like a metallic surface. When using ASTM B193 for conductive materials, a smooth surface is assumed due to the nature of metallic surfaces. The variations at the interface of the conductive layer and substrate introduce error into the resistivity measurement. This would lead to variations in both a bulk and lateral resistivity due to the variation in thickness at the interface.

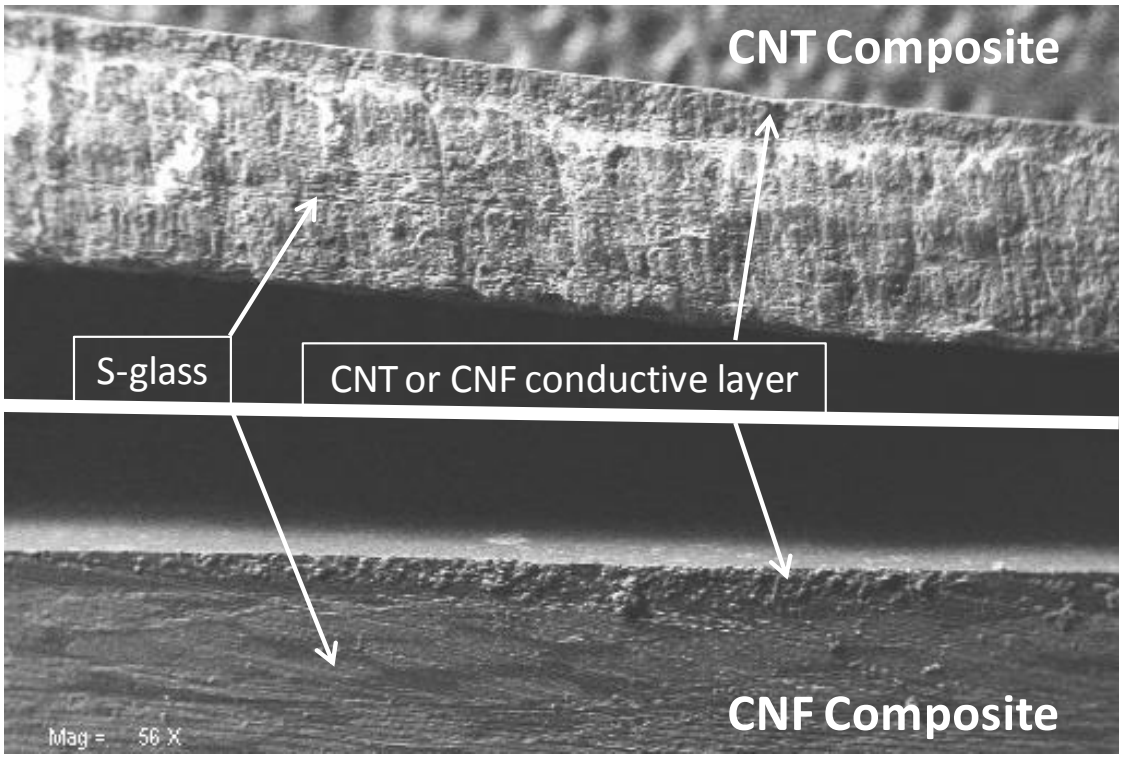

Figure 7. SEM image of both the CNT (top) and CNF (bottom) samples. The CNT and CNF conductive layers are on top of the S-glass substrate. The CNT and CNF layers are both a nominal 150 µm, while the S-glass is a nominal 900 µm.

The CNF composite was provided by Applied Sciences, Inc. The actual CNF's are dispersed in 5250-4 epoxy resin on top of 6781 S-glass laminate. The entire sample is 1 mm thick with the CNF and resin layer being a nominal 150 µm thick. The CNF's contained in the epoxy resin are estimated to be 100 nm in diameter and up to 100µm in length. The CNF layer contains 20 gsm of CNF's [13].

As shown in Figure 8, the CNF composites are manufactured with a distinctly different structure than the CNT's. The CNF has a "stacked-cup" morphology base that is precipitated from a nanoscale catalyst particle. The stacked-cup structures consist of sheets of graphene arranged in a structure resembling concentric cylinders. The CNF's

are much different than the CNT samples in both growth technique and dimensions; however they exhibit similar properties as a multi-walled CNT. The primary benefit of a CNF is the much lower cost with fewer processing issues during fabrication. Figure 8 displays the PR-25 type of CNF. The CNF is available in a variety of types and grades which vary in wall thickness and crystalline structure [6].

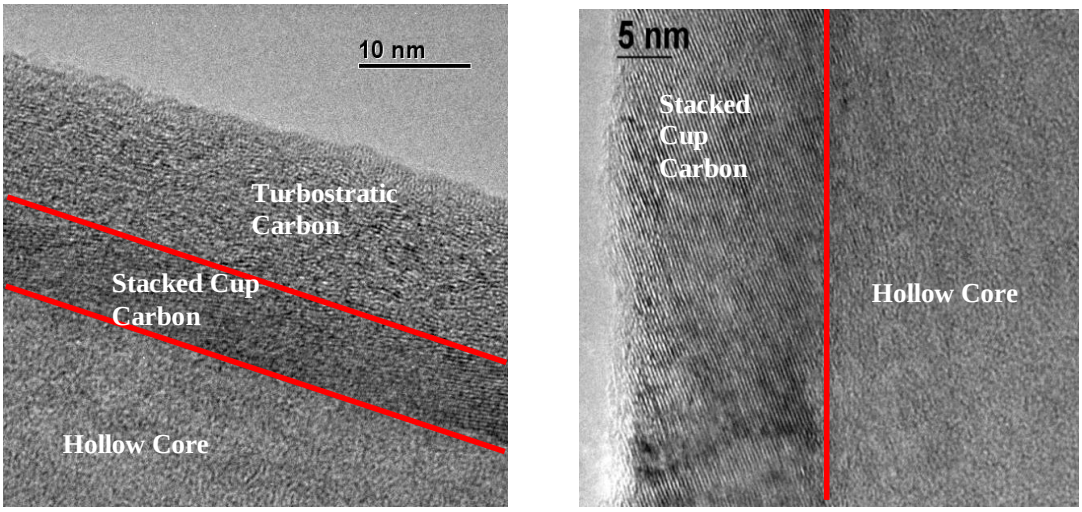

Figure 8. The transmission electron microscope (TEM) image on the left represents a typical PR-19 carbon nanofiber with a large fraction of turbostratic carbon deposited on the catalytic layer (stacked-cup carbon). The catalytic carbon layer is carbon precipitated from the catalyst particle while the turbostratic layer is added through chemical vapor deposition techniques. The image on the right is typical of PR-25 fiber that only has the catalytic carbon layer [6]

2.1.3 Radiation Damage

In a composite material, the radiation damage occurs in both the conductive nanofiller material and in the epoxy resin. The measured changes in resistivity of the nickel nanostrand composites following electron irradiation were determined to be due to chemical changes in the epoxy resin. [1] However, x-ray absorption fine structure (XAFS) measurements found little evidence to support the epoxy resin chemical changes

[2]. [2] reported no increase in oxide formation following electron irradiation. XAFS measurements are a spectroscopic technique that uses x-rays to probe the physical and chemical structure of a material at an atomic scale. The x-rays are chosen to be at and above the binding energy of an electron level of a particular atomic species. This allows for the identification of specific atomic particles present in a material.

When considering the CNT and CNF composites, the conductive materials are comprised of carbon. Carbon is a semi-conductive material and extensive research has been conducted on similar semiconducting material such as silicon. This research can provide a basis for radiation effects for the CNT and CNF conductive nanoparticles.

This research is primarily focused on the damage caused by electrons and neutrons. As shown in Figure 9, the two main effects are ionization and non-ionizing radiation effects. The primary effect of ionizing radiation is the creation of electron-hole (e-h) pairs which elevates a valence electron into the conduction band. If the incident radiation energy is high, the ionization could lead to free secondary electrons which would continue to create e-h pairs and move throughout the material [14].

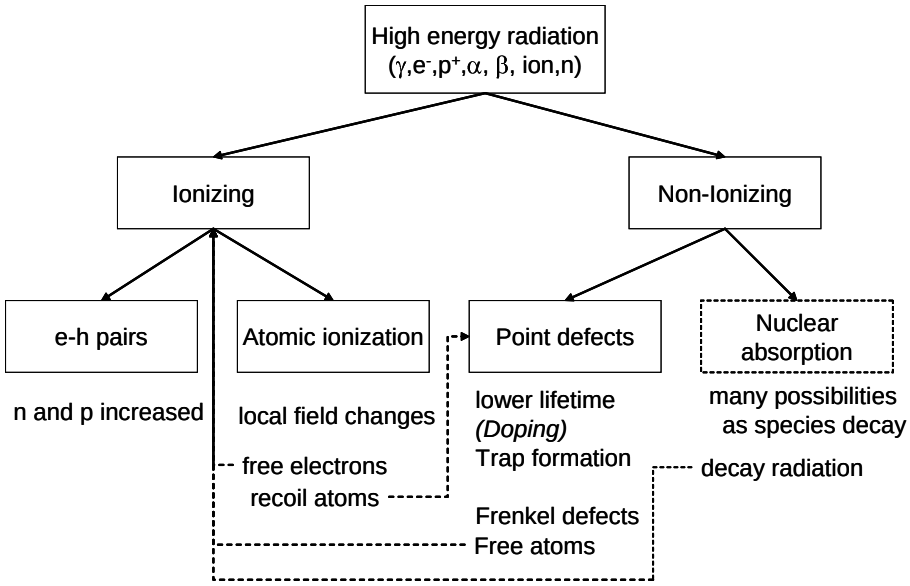

Figure 9. Radiation effects can be divided into two broad categories of ionizing and non-ionizing radiation. However, as shown, the effects are interconnected [14].

Also shown in Figure 9, the second effect of radiation is non-ionizing, which includes nuclear absorption and creating point defects. Point defects are caused by incident radiation transferring its energy to the atom and dislocating it from its lattice site. This dislocation can lead to a reduction in carrier mobility, carrier lifetime and trap formation. If the incident radiation is high enough in energy, it can undergo nuclear absorption which can lead to a variety of secondary radiation, including gammas, alphas, protons, and betas. Generally, non-ionizing radiation can lead to the creation of point defects that may reduce the conductivity of the material. [14]

Due to the high flux of gammas in the OSURR, photon damage mechanisms must be taken into account. The primary damage mechanism of photons is ionization through the photoelectric effect (PE), Compton scattering (CS) and pair production (PP). While the secondary damage mechanism of photons are non-ionizing effects, due to the zero

rest mass of photons. PE, CS, and PP all result in the creation of charged particles. Once the charged particles are created, the effects of the created particle will be analogous to the following description of electrons [14].

In this investigation, the CNT and CNF composites were exposed to the two types of radiation, neutrons and electrons. Since the Ohio State University Research Reactor (OSURR) was the source of the neutron radiation, they were also exposed to a large gamma flux. Therefore, the effects of gammas must be taken into consideration for our composite materials. The basic mechanisms can be classified by radiation type. First, the primary damage mechanism of neutrons is non-ionizing effects. Therefore, incident neutrons cause atomic displacements within the lattice and reduce the conductivity of the composite material. Due to the uncharged nature of a neutron, no coulomb force interacts on the neutron. Therefore, neutrons have a low cross section for interaction and penetrate deep within the material. The depth of penetration is dependent upon the incident neutron energy.

The primary and secondary mechanisms associated with electrons are energy dependent. Therefore, both ionizations and non-ionizing effects are associated with electron radiation. The non-ionizing effects will also lead to atomic displacements and a reduction in conductivity analogous to the neutron non-ionizing effects. The ionizations will lead to excitation of valence electrons creating e-h pairs [14].

However, the lower atomic mass of electrons as compared to neutrons needs to be taken into account when attempting to predict the atomic displacements. The electron has an atomic mass of $9.11\times10^{-31} kg$, while a neutron has an atomic mass of $1.68\times10^{-27} kg$. Therefore, the neutron is 1.8×10^{3} more massive than the electron. The

negative charge associated with electrons creates a Coulomb force. This Coulomb force affects the cross section for interaction within the material. Therefore electrons penetrate deep within the material. However, despite the larger mass of a neutron, due to the lack of a Coulomb force the neutrons will penetrate further into the material at a given energy [15].

Once radiation damage occurs, a neutralization process can follow. Neutralization is temperature and applied electric field dependent in most semiconducting materials [14]. In most semiconducting materials such as silicon displaced atoms are referred to as Frenkel pairs. The vacancy at the atom's previous location and the interstitial where the atom re-attached to the lattice are termed a Frenkel pair. The Frenkel pairs are known to recombine at temperatures below RT. In metallic materials, displaced atoms can recombine at all temperatures. It has been observed that defects inside CNT's need high temperatures to facilitate the recombination. The high temperature increases the mobility of the interstitial atoms to recombine in the vacancies. The increased mobility allows for faster annealing through forming a non hexagonal structure [16].

2.2 Previous Research

Nickel nanostrand composites were researched by [1] and [2]. The results of [1] and [2] are inconsistent. Table 2 and Table 3 show the surface resistivity results on electron irradiations of nickel nanostrand composites by [1] and [2]. Two main differences in the reported values are the magnitude of the pre-irradiation resistivity

values, and second the direction and magnitude of the change in resistivity with the post irradiation resistivity values.

Table 2. Reported surface resistivity values by [1] for nickel nanostrand composites. The reported changes due to electron radiation ranged from 45-440% depending on the configuration.

Configuration		Pre-Irradiation		Post Irradiation		Change
		Mean Resistivity	1-σ [mΩ-cm]	Mean Resistivity	1-σ [mΩ-cm]	%
Ext		20.0	±0.2	108	±1.0	+440
D		10.6	±0.3	37.2	±1.9	+250
M		12.5	±1.2	38.9	±1.9	+211
I		13.9	±0.1	35.1	±1.8	+152
B		22.9	±0.5	49.5	±2.5	+116
C		25.6	±1.8	45.3	±2.3	+76.9
A		30.3	±0.8	44.0	±2.2	+45.2

Table 3. Reported surface resistivity values by [2] for Nickel nanostrand composites pre and post electron irradiation. [2] reported a change in resistivity in the opposite direction as [1].

Pre-Irradiation Measurements					Post Irradiation 2 x 10^{16} cm^{-2}			
						68% Interval		
Sample	Dot Alignment	Average Measured Resistance [mΩ]	Minimum [mΩ]	Maximum [mΩ]	Average Measured Resistance [mΩ]	68% Interval Lower Limit	68% Interval Upper Limit	Relative Change in Mean Value [%]
Ni-36-1	up	135.5	132.7	139.7	129.0	124.9	136.4	**-4.8**
Ni-36-1	down	155.7	150.2	159.4	154.2	149.8	160.1	-1.0
C-36-2	up	184.4	180.7	186.5	153.7	152.8	154.5	-16.6
C-36-2	down	168.7	166.2	170.1	142.2	140.3	144.6	**-15.7**
C-3-5	up	160.0	156.2	165.8	149.1	145.9	154.2	**-6.8**
C-3-5	down	157.0	147.0	165.9	138.4	125.8	149.6	-11.8
Ni-3-1	up	195.3	191.7	197.4	168.0	164.9	170.8	-14.0
Ni-3-1	down	181.7	180.8	182.5	162.3	158.2	166.3	**-10.7**

First, the magnitude of the pre-irradiation values reported by [1] and [2] can be accounted for in the size of samples each used to conduct a four point collinear resistivity

test. Both [1] and [2] used the same sized samples, however, [2] applied a correction factor to the resistivity calculations due to edge effects and thickness to probe spacing effects. The correction factors were applied based on [18]. [1] did not use the correction factor and if the same correction factors were applied to the reported values of [1], they would match more closely with the reported values of [2].

There are three types of correction factors that can be applied to a four point probe measurement. The first is for sample thickness, the second corrects for lateral sample dimensions, and the third corrects for sample edges effects[18]. All samples in this investigation were approximately 5 x 25 x 1 mm. The probe spacing was maintained at 6.35 mm, this allows for the thickness (t) to be less than the probe spacing (s), and the width (w) to be larger than s. The dimensions described above for the test fixture and composite samples allow for no correction factors to be applied to the four point measurements on the CNT and CNF composite samples.

[1] reported an increase in resistivity post electron irradiation while [2] reported a slight decrease in resistivity. This could be accounted for by the type of samples tested. [1] tested 8 different configurations of the nickel nanostrand, while [2] only tested one configuration. In addition, [1] samples consisted of two types of epoxy, RS-3 space grade epoxy and aero epoxy. The resistivity is believed to be dominated by the type of epoxy and the percent loading of the nanofiller. Therefore, different epoxy's will result in different resistivity's due to the need to tunnel from nanostrand to nanostrand along the conductive path. The radiation affects on the epoxy becomes just as important as the radiation effects on the conductive material.

The previous research studies are the primary sources for comparison. However, additional radiation effects research on non-polymerized CNTs and CNFs will be used for comparison. [16] conducted research into the electron radiation effects on CNTs. In the research, a TEM was used to irradiate individual CNT's and also to look at images of the CNTs as they were irradiated. It was discovered the electron beam would cause a deformation of the individual CNTs. A high temperature anneal was also observed.

[19] researched the effects of electron beam radiation on CNF's. [19] used atomic force microscopy (AFM) to observe the morphology of the CNF's. The AFM images produced pre and post electron irradiation by [19], showed both a bending and fusing of adjacent CNFs. It should be noted that the breaking of a CNF would more than likely decrease the conductivity if they were in a polymerized composite, while the fusing of adjacent CNFs would increase the conductivity of the CNF composite. [19] described the fusing process as a welding process. This would lead to electrical transfer from one tube to the next.

2.3 Summary

The three types of composite materials under investigation are nickel nanostrand, CNT and CNF composite materials. The nickel nanostrand radiation effects have already been explored and they will be compared to the CNT and CNF composites. The resistivity will be the primary electrical property used to investigate the radiation effects. The resistivity of the material is an important electrical property in satellite structures. Maintaining a low resistivity will provide protection from the space radiation

environment. If a resistive material is used to replace aluminum in satellite structures, they will be susceptible to electrostatic discharge.

The effects of neutron and electron radiation will be the primary focus. Therefore, this will lead to both ionizing and non-ionizing damage mechanisms within the composite materials. The space radiation environment will be defined by MIL-STD-1809. Specifically the electron radiation environment will be simulated. In addition to the space radiation environment, the composite materials will be exposed to higher dose levels of both electrons and neutrons to facilitate the analysis of radiation effects on the conductivity.

III. Experiment

3.1 Experiment Overview

In this research, the changes in resistivity on three types of composites under a simulated space radiation and thermal environment were investigated. The three sample types include nickel nanostrand, carbon nanotube, and carbon nanofiber. Resistivity and ESD measurements were conducted on CNT and CNF composites irradiated with reactor neutrons, and 0.5 MeV electrons using a Dynamitron accelerator. In addition, resistivity measurements were conducted on nickel nanostrand, CNT, and CNF composites that were thermally cycled. Post-irradiation ESD measurements were performed, while post-irradiation and post-thermal cycle resistivity measurements were performed.

3.2 Sample Preparation

The samples were cut from a 610 x 610 x 1 mm sheet composite. The samples were cut in order to fit the resistivity measurement fixture (5 x 25 x 1 mm). Samples cut for a corresponding mechanical composite research project were cut from the same composite sheets. Therefore, the samples used for this experiment were not cut adjacent to one another. Rather, they were cut from different portions of the larger sheet. This explains the lack of uniformity of the nanofiller spread throughout the epoxy resin in one of the sheets. Non-uniformity of the nanofiller would result in a difference in resistivity values between samples due to a different epoxy-to-nanoparticle volume within each test sample.

The samples were cut using a diamond saw. The number of samples cut of each type are given in Table 4. As indicated in Table 4, separate samples were cut for the

neutron irradiations and thermal cycling experiments. A micrometer was used to measure the thickness of the nickel nanostrand samples. Due to the S-glass insulating substrate on the CNT and CNF composite, a scanning electron microscope was used to determine the thickness of the conductive layer for the CNT and CNF composite.

Table 4. Number of samples cut from the composite sheets of each type and the associated experiment each sample was used for.

	Neutron Irradiation	Electron Irradiation	Thermal Cycle
Carbon nanotube	4	2	1
Carbon nanofiber	4	2	1
Nickel Nanostrand - control	0	0	2
Nickel nanostrand-external	0	0	2

3.3 Resistivity Measurements

3.3.1 Test Setup

Resistivity measurements were performed using the four-point collinear probe resistivity configuration using [20]. ASTM standards B193-02 [21], D4496-04 [22] and D257-07 [23] were used for surface and volume resistivity. For most materials, only one ASTM standard would be followed. However, due to the conductive nanofillers incorporated into the insulated epoxy, elements from all three ASTM standards were followed. This four-point probe technique was accomplished using a measurement fixture connected to a Keithley model 4200 Semiconductor Characterization System (SCS). Figure 10 shows the test system for the surface and volume resistivity

measurement. The test fixture is contained inside an aluminum box which acts as a faraday shield to reduce electromagnetic interference while taking measurements.

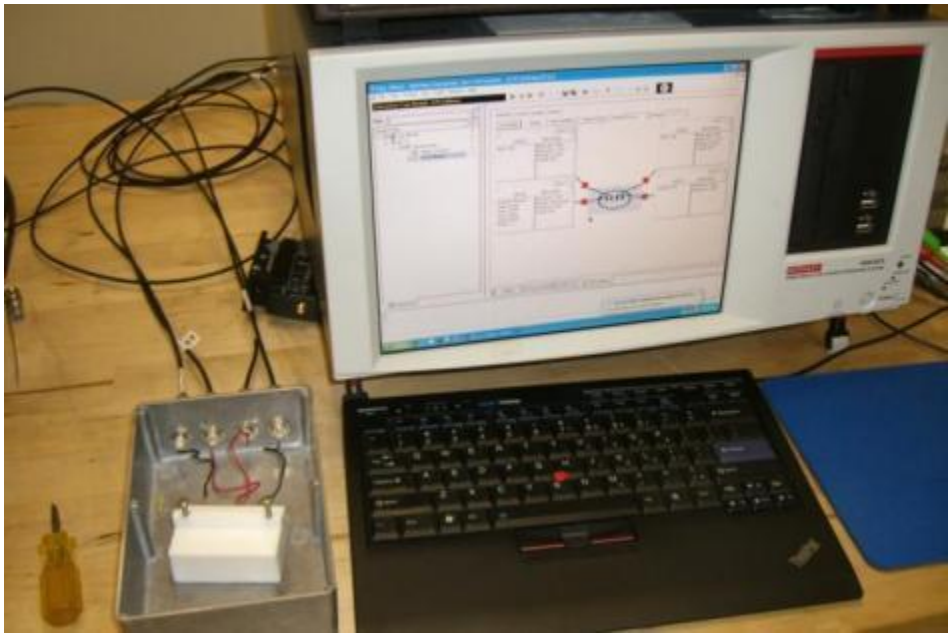

Figure 10. Surface resistivity test setup. Test fixture is attached to the Keithley 4200 SCS. A KITE program was used to vary the current source and measure the voltage difference between probes 2 and 3.

The test fixture was designed to maintain a constant probe distant between measurements. The test fixture is made from high density polyurethane (HDPE) and has four gold probe contacts that connect to the sample under test. Each gold probe is spaced a distance of 0.635 cm apart from adjacent probes. The four gold probes are connected to 7078-TRX-10 low noise triax cables which are connected directly to the corresponding signal measuring unit (SMU) on the Keithley 4200 SCS.

Measurements were taken by sourcing current through probe 1 and measuring the voltage drop between probes 2 and 3. Probe 4 was connected to ground via the Keithley 4200 force ground. The current injected into probe 1 was varied between -10 to +10 mA

in 1 µA increments, alternating positive and negative currents with two measurements at each current too reduce the Johnson noise [20]. Measurements were taken at a three-second sweep delay, followed by a three-second hold time to allow current relaxation across the surface between measurements.

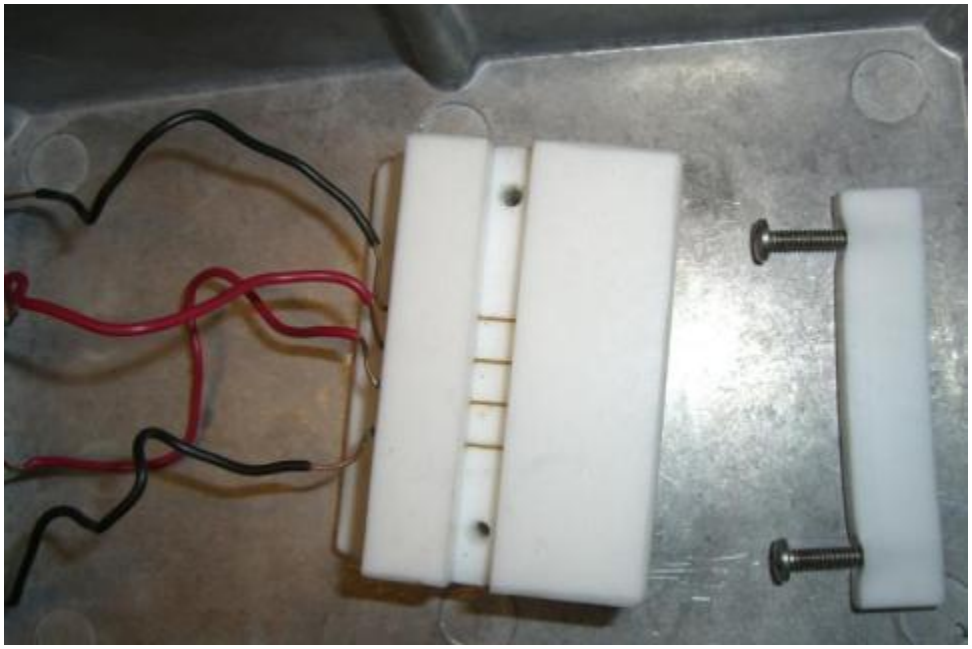

Figure 11. Close up image of the test sample fixture with the gold contacts. The gold contacts are fixed into the test fixture to maintain a constant probe distance between measurements. The compression clamp is shown lying next to the fixture which was used to ensure probe contact into the conductive surface of the nanoparticle layer.

Sample resistivity was found by using the measured sample resistance and multiplying it by the effective length. The sample resistance was found using Ohm's law as shown in equation (1).

$$R = \frac{\Delta V}{I} \quad [\Omega] \tag{1}$$

In equation (1) ΔV is the measured voltage difference between probes 2 and 3, and I is the current sourced to probe 1. In order to find the sample resistivity, the sample resistance is then multiplied by the effective length. The effective length can be defined in one of two ways. The first is to find volume resistivity. The effective length is defined as $\frac{wt}{s}$ where w is the width, t is the thickness and s is the probe spacing. The effective length when multiplied by the resistance will determine volume resistivity. Therefore, the volume resistivity can be found by equation (2) [20].

$$\rho_v = \frac{\Delta V}{I} * \frac{wt}{s} \quad [\Omega - cm] \tag{2}$$

In addition to the volume resistivity, the effective length is used to determine surface resistivity. The surface resistivity can be determined by multiplying the resistance by the effective length defined as $\frac{w}{s}$. The surface resistivity has units of ohms but is commonly referred to in units of Ω/square. The surface resistivity can be found by equation (3) [21].

$$\rho_s = \frac{\Delta V}{I} * \frac{w}{s} \quad [\Omega / square] \tag{3}$$

The four point collinear resistivity measurement technique reduces the probe resistance, contact resistance and spreading resistance that are characteristic in a two probe resistance measurement [18]. The calculated resistivity's are compliant with ASTM B193 [21].

The inverse of the resistivity is conductivity. Therefore, in order to find the conductivity of a material using the resistivity, equation(4) can be used [17].

$$\sigma = \frac{1}{\rho} \tag{4}$$

Conductivity can be expressed in terms of volume conductivity, or surface conductivity analogous to volume and surface resistivity. The units of volume conductivity are Siemens/cm, while the units of surface conductivity are Siemens/square [23].

3.3.2 Measurement Procedures

Each sample was prepared as discussed in section 3.2 and then cleaned and allowed to dry. The sample was placed in the test fixture and held in place with the compression clamp. Once the sample was in place, the top of the aluminum cage was secured and the Keithley 4200 SCS was used to obtain the current-voltage (IV) measurements between -10 to +10 mA using the Keithley Interactive Test Environment (KITE). An example of a CNT composite *IV* measurement is shown in Figure 12. Also shown in Figure 12 is the linear regression line through the data with the slope which is equal to the resistance of the sample according to equation (1). This resistance is in units of ohms. In order to obtain the resistivity, the slope is multiplied by the effective length according to equation (2) or equation (3).

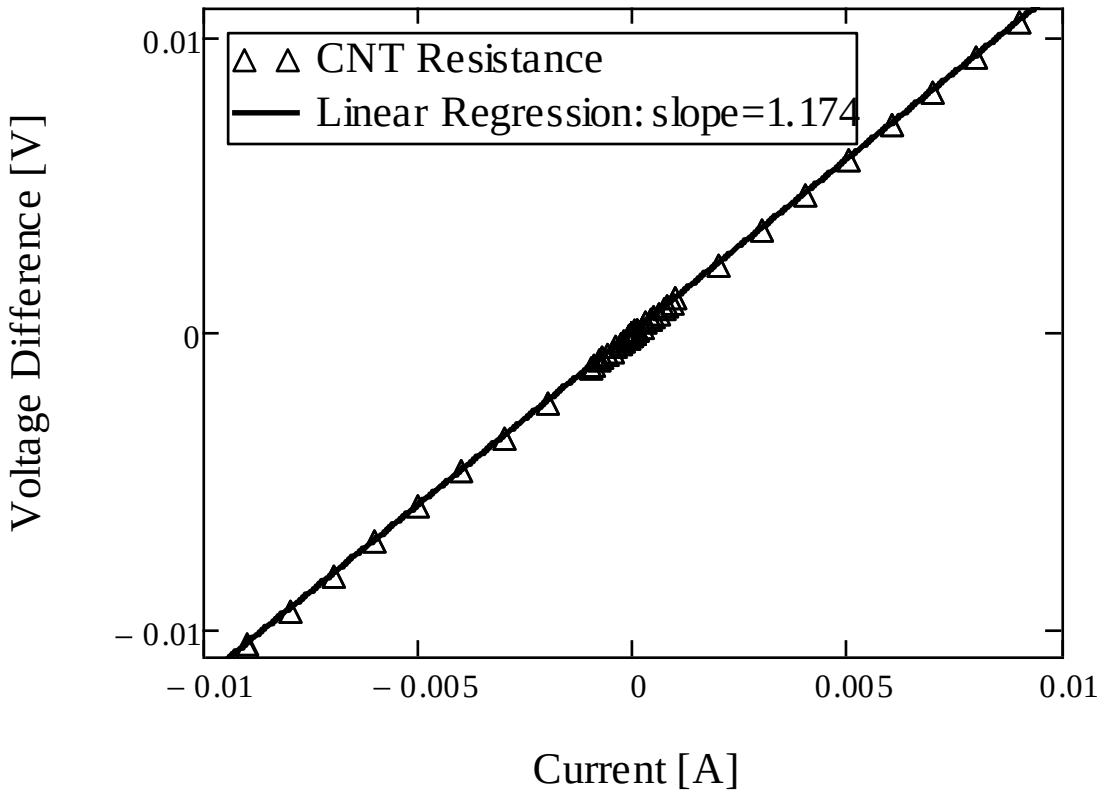

Figure 12. *IV* measurement of the CNT sample plotted with the linear regression line. The slope of the line is the resistance of the sample according to equation (1).

During the early stages of measurements, it is believed the compression clamp was not secure enough and the gold probes were not making contact with the conductive layer. This resulted in a non-linear response between the voltage difference and the varied current source. As shown in the SEM images of the samples, the nanofiller/epoxy layer is not smooth. A few techniques were explored to resolve this problem, however the best solution was increasing the pressure with the compression clamp. This compensated for the lack of smoothness in the sample, by ensuring the gold probes pushed through any epoxy layer and got close enough to the conductive pathway the

nanoparticles provided. A screw driver was used to secure the compression clamp to ensure maximum probe contact with the conductive layer. This may introduce some error in the measurement because the compression clamp was not secured consistently for each measurement. In addition, the screws were made of metal while the test fixture was made of HDPE which loosened over time, resulting in inconsistent compression clamp pressure.

3.4 Electrostatic Discharge Test

A transverse (bulk) resistivity measurement was desired for the CNT and CNF composites. However, due to the S-glass insulating substrate for the CNT and CNF composites, it was not possible. Therefore, [1] introduced an electrostatic discharge test which was correlated to resistivity. The ESD test was conducted on the CNT and CNF composites pre and post neutron irradiation to investigate the feasibility to measure the transverse resistivity of the CNT and CNF composites despite the insulating S-glass substrate.

The test system of [1] was replicated as much as possible, as shown in Figure 13. Figure 14 shows the equivalent test circuit designed by [1]. The ESD3000 was used as the discharge source exclusively. The ESD3000 charged to the desired output voltage, the pointed contact discharge tip of the ESD3000 was placed on the sample prior to discharge. The discharge ground contact lead of the ESD3000 was connected to the SDN-414-025 current viewing resistor which was then connected to the Tektronic 5104B oscilloscope that captured the current waveform for analysis. The current waveform output captured by the oscilloscope was noisy and hard to analyze.

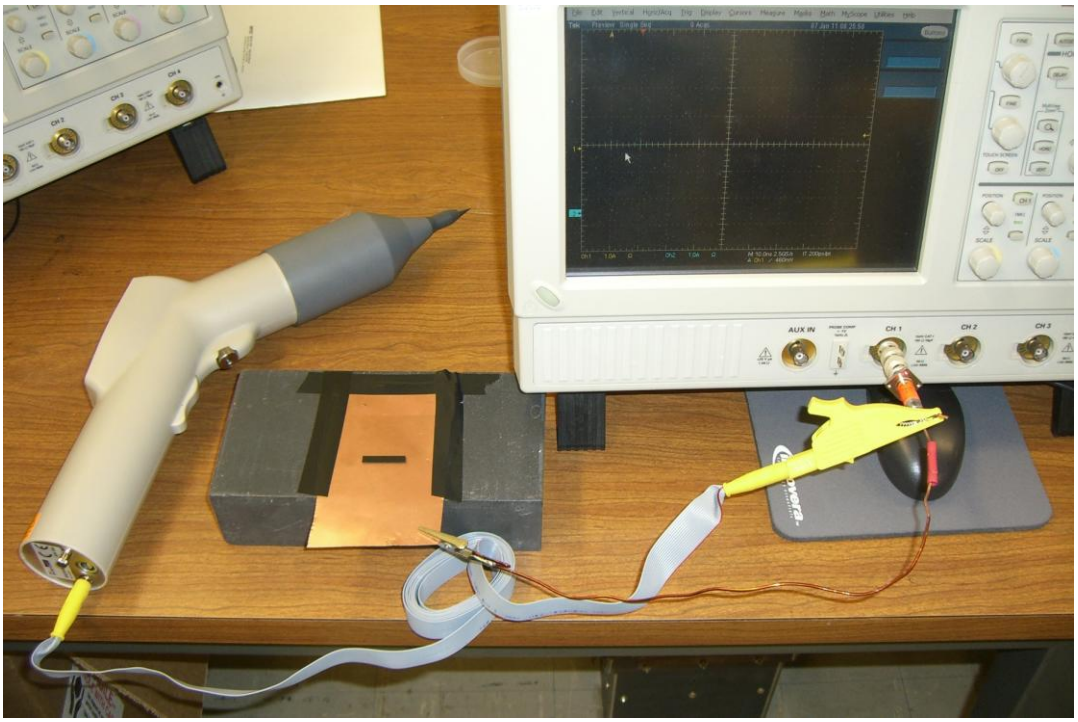

Figure 13. ESD test setup showing the ESD3000 discharge source, sample under test, SDN-414-025 current viewing resistor, tektronic Oscilloscope, cooper wire, copper plate and rubber brick.

Due to the noisy output inherent with the waveform, a smoothing routine was applied to the waveform for a more desirable current waveform. The signal was smoothed using a localized linear best fit routine. Figure 15 shows an example of a typical 12 kV smoothed current waveform output. An example of the actual current waveform and the associated smoothing routine waveform is shown and described in Appendix B.

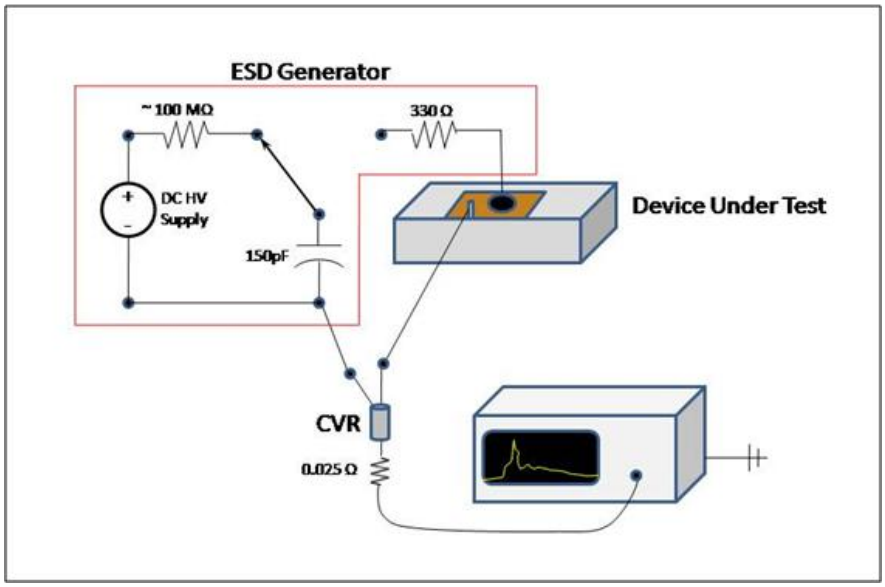

Figure 14. Equivalent circuit for ESD test showing ESD3000 generator, Device under test, current viewing resistor connected to the oscilloscope [1].

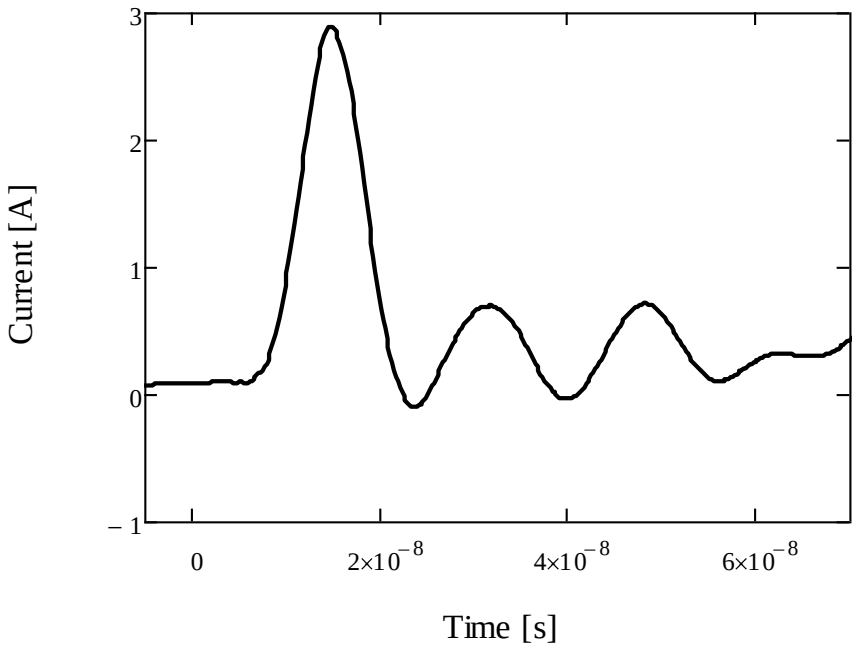

Figure 15. Typical smoothed current waveform output for a 12 kV voltage discharge.

[1] designed the ESD measurement to simulate the discharge of surface charge buildup associated with resistive material in space. Discharges were conducted over a wide range of voltages. The discharge voltages initially were conducted at 2 kV, 4 kV, 8 kV and 12 kV. The output current waveform was recorded at each discharge voltage and compared to the expected current waveform specified in [24]. Figure 16 shows the expected output current waveform with associated parameters of interest [24].

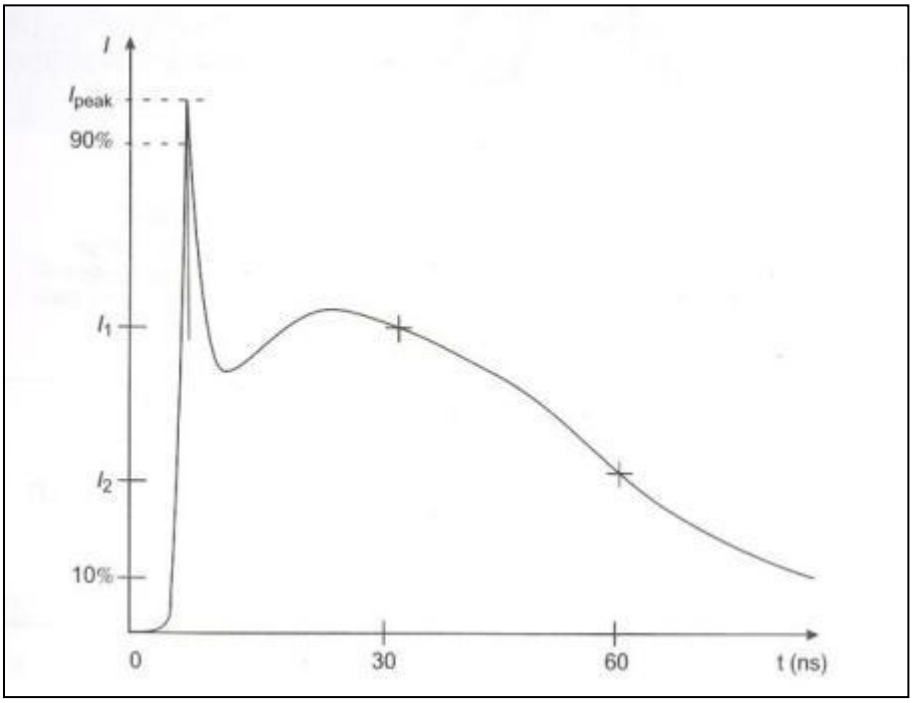

Figure 16. Current waveform of typical ESD baseline pulse where t_r is pulse rise time from 10 percent to 90 percent of I_{peak}, I_1 and I_2 are 30 and 60 ns current amplitudes respectively. [24]

The 12 kV discharge voltage was most consistent and similar to the expected current waveform and used for investigation and analysis. The waveform generally contains a fast rise to a peak current within the first 10 ns, with an associated fast current

decrease with an associated gradual rise to a much lower peak current with an oscillating current decrease.

Figure 16 shows the expected parameters of interest as I_{peak}, I_1 and I_2. I_1 and I_2 are the current amplitude at 30 and 60 ns respectively. Figure 15 shows the typical waveform for the CNT and CNF composite, and the best parameter of interest to analyze the waveform would be the I_{peak} and the rise and fall time of the first peak. Due to the insulating properties of the S-glass substrate, I_1 and I_2 parameters would not provide useful information. The current amplitudes associated with I_1 and I_2 are useful in the analysis of completely semiconducting material. Once the initial ESD shock is complete, the insulating S-glass material cuts the extended flow of any current through the sample. The high breakdown voltage of the S-glass does not allow current to flow long enough to use the I_1 and I_2 parameters for analysis.

3.5 Irradiations

3.5.1 Overview

Both neutron and electron irradiations were conducted on the CNT and CNF composites. The initial fluence for the electron irradiation simulated a 35 year lifecycle of a satellite in geosynchronous orbit, as defined by MIL-STD-1809. The initial neutron irradiation simulated the electron NIEL effects of a 35 year space radiation environment in geosynchronous orbit. After each electron and neutron irradiation, a second irradiation was conducted at a much higher fluence level. The second electron irradiation increased the electron fluence from $1x10^{16}$ to $6x10^{16} e^{-}/cm^2$. The second neutron irradiation

increased the neutron fluence level from $1.11x10^{14}$ up to $4x10^{16} neutrons/cm^2$ with 4 fluence levels in between.

3.5.2 Electron Irradiation

Electron irradiations were conducted using 0.5 MeV electrons in a 1.5 MeV Dynamitron Electron Accelerator. For all irradiations, 0.5 MeV electrons were used. For the first irradiation, the CNT and CNF samples were irradiated to a fluence of $1x10^{16} e^{-}/cm^2$. This fluence and energy was used to match the electron irradiations used by [1] and [2]. This fluence level follows the space flux defined by MIL-STD-1809 as $8x10^{6} e^{-}/cm^2 s$ as shown in Table 1. However, the beam current varied between 3 to 5 μA for the first irradiation, and total Coulomb count was 1396 counts according to equation (5).

The electron energy of 0.5 MeV was used for comparison of the nickel nanostrand samples irradiated by [1] and [2]. Through CASINO simulations for the CNT and CNF samples, the 0.5 MeV electrons will penetrate through the CNT and CNF conductive layer and deposit the majority of their energy in the S-glass substrate. Thus, the damage mechanism caused by the 0.5 MeV electrons will be dominated by atomic displacements. Figure 17 shows the Casino simulation. The contour lines represent electrons losing energy. Therefore, a majority of the electron energy is lost within the S-glass substrate.

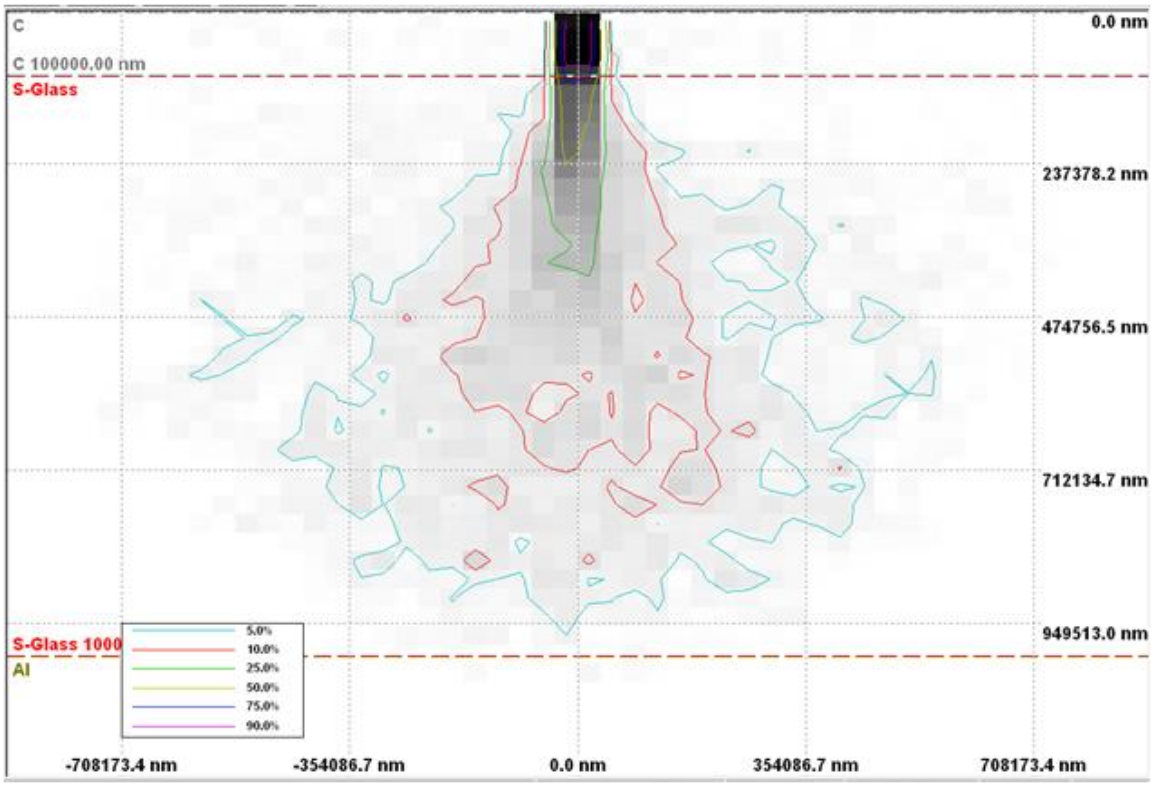

Figure 17. CASINO simulation for electron deposition incident on the CNT and CNF composites.

The operating parameters used for the Dynamitron are electron energy, beam current, and total Coulomb count. As discussed above, the electron energy used was 0.5 MeV. The Coulomb count was determined according to equation(5) to ensure the correct electron fluence was achieved.

$$Coulomb\,Count = \frac{Desired\ Fluence \times Charge\ per\ Electron \times Beam\ Area}{Full\ Scale\ Factor} \qquad (5)$$

The charge per electron is $1.602\,x10^{-19}$ C, the beam area was 5.228 cm^2 and the full scale factor was 6 μA. Through the use of equation (5) and using the recorded parameters, a fluence of $1x10^{16} e^{-} / cm^2$ was found as the fluence delivered to both the CNT and CNF composite samples. The first irradiation lasted 35 minutes. Therefore, an average flux of

$4.8 x 10^{12} e^{-} / cm^2 s$ was delivered to the composite samples during irradiation. There were minor fluctuations in the electron beam from the Dynamitron, however, the beam maintained a fairly constant flux.

The beam area had a circular collimator and covered 522.8 mm^2, this corresponds to a circular beam diameter of 25.8 mm wide. With the samples being 5 mm wide and 25 mm long, both CNT and CNF composites could be placed side by side on the cold head and irradiated simultaneously. Figure 18 shows the mounting method used for the CNT and CNF composite samples. Vacuum grease was used to attach the samples to the copper cold head. In addition, two pieces of scotch tape were placed at each end of the sample to ensure the samples were secure.

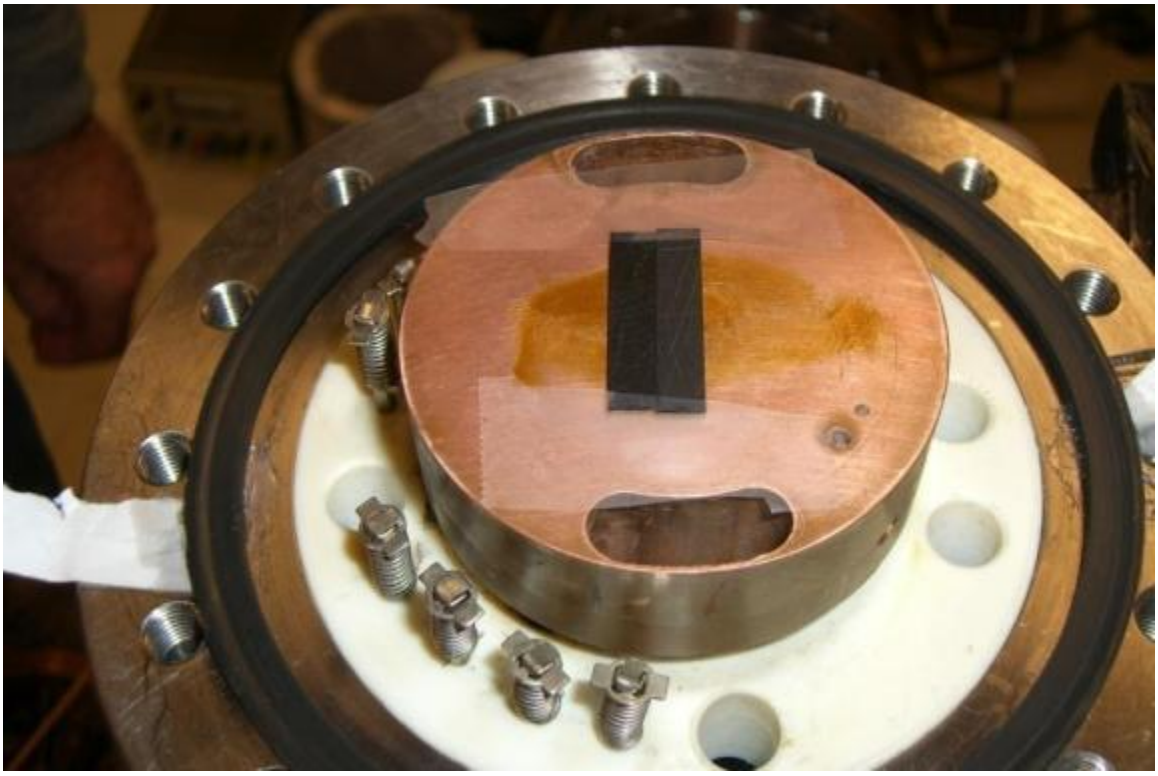

Figure 18. Picture of the CNT and CNF composite samples on the copper cold head. The electron beam area covered the entire area of the samples. The cold head was water cooled to keep the samples at room temperature.

The cold head was then attached to the end of the beam line and electrically isolated. The cold head was water cooled to ensure the samples were maintained at room temperature and in order to prevent any thermal damage from the electron beam. The beam line was placed under vacuum to a level of 10^{-7} torr. Figure 19 shows the cold head attached to the end of the beam line with water flowing through the cold head to maintain a constant room temperature. To ensure a uniform irradiation across the entire beam area the beam was continuously altered across the samples. The Dynamitron uses steering and scanning techniques to accomplish the uniform beam. For this irradiation, the steering was accomplished in both the x and y cardinal directions. However, only the x direction

had an operative scanning device installed. Therefore, through beam characterization analysis, the beam appeared to have a uniform beam diameter. However, due to the inoperative y scanner, some non-uniformities may have been present.

Figure 19. Picture of the Dynamitron with the cold head attached to the end of the beam line. The cold head is electrically isolated and pumped to a vacuum level of 10^{-7} torr. Water flows through the cold head to maintain the samples at a constant room temperature.

After the first electron irradiation, the samples were removed from the cold head, cleaned and post irradiation resistivity measurements were taken. The same samples were then irradiated by the same method discussed above to a fluence of $6x10^{16} e^{-}/cm^{2}$. In order to achieve this higher dose, the Dynamitron was run different. A full scale factor of 2 μA, while the beam current operated between 0.1 to 0.2 m*A* was used to achieve the higher dose. This resulted in a higher flux delivered to the samples during

the second irradiation. Through equation (4) the total coulomb count achieved was 2093 C. The second irradiation took 87 minutes to complete. Therefore, the flux for the second irradiation was $9.5 x 10^{12} e^{-} / cm^2 s$. Table 5 summarizes the operating parameters for each irradiation.

Table 5. Summary of the fluence levels for each irradiation with the associated Dynamitron operating parameters.

	Fluence [e^-/cm^2]	Flux [e^-/cm^2-s]	Coulomb Count [C]	Beam Area [cm^2]	F.S. Factor [μA]	Beam Current [μA]	Vacuum [torr]
Irradiation # 1	1×10^{16}	4.8×10^{12}	1396	5.228	6	3-5	10^{-7}
Irradiation # 2	6×10^{16}	9.5×10^{12}	2093	5.228	2	100-200	10^{-7}

3.5.3 Neutron Irradiation

Neutron irradiations were conducted at the Ohio State University Research Reactor (OSURR). The OSURR is a pool-type reactor that operates continuously at full power up to a maximum of 500 kilowatts. The average thermal neutron flux in the core is approximately $5 x 10^{12} neutrons / cm^2 s$. The facility has several beam ports that can be used to insert samples for irradiation. The central irradiation facility (CIF) and a pneumatic transfer tube referred to as the "rabbit tube" were utilized to irradiate the CNT and CNF samples. Figure 20 shows a picture of the core of the OSURR with the associated beam ports.

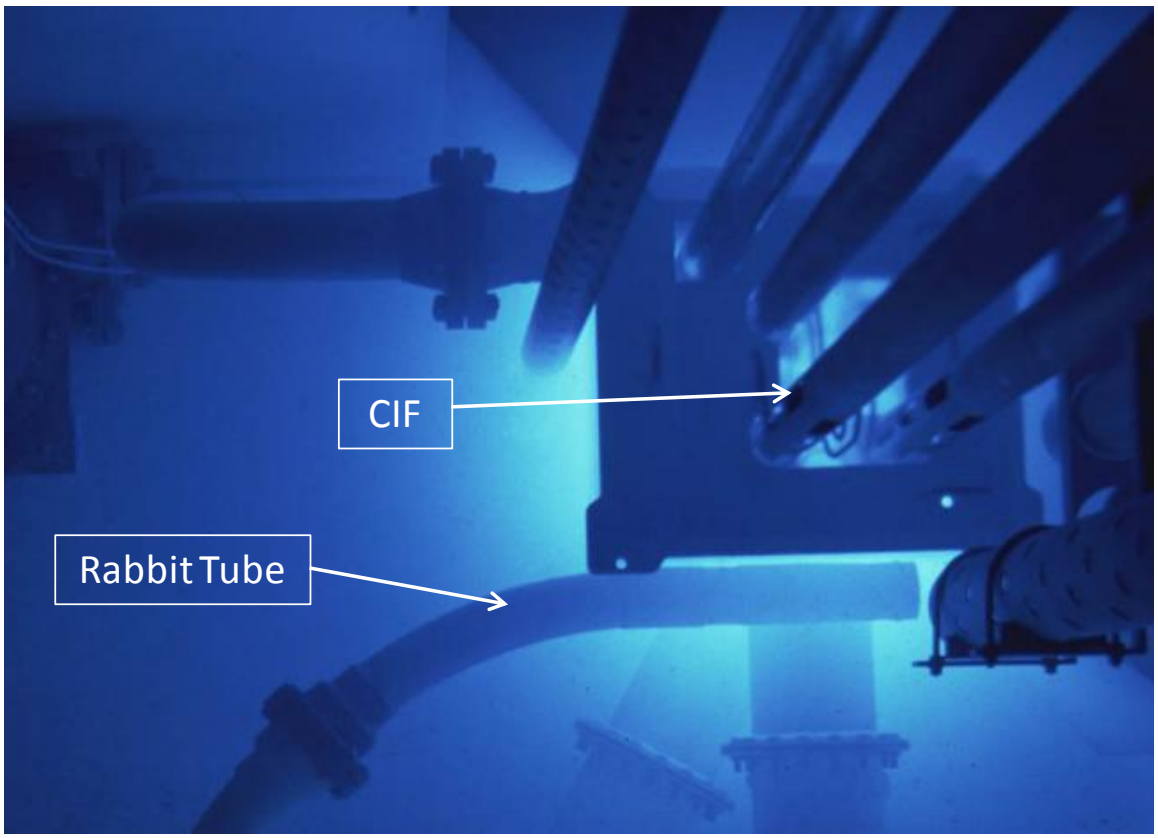

Figure 20. Depiction of the OSURR core with the associated beam port. The two beam ports used in the neutron irradiations are the pneumatic transfer tube "rabbit tube" and the central irradiation facility (CIF). [27]

The rabbit tube was used for the initial neutron irradiation. The rabbit tube provided a 1 MeV equivalent fluence of $1.11 x 10^{14} neutrons / cm^2$. The samples were first wrapped in a cotton cloth and then again wrapped in cadmium in order to shield from thermal neutrons. Figure 21 depicts the cross section for cadmium as a function of neutron energy. At energies below approximately 0.2 eV, the cross section is 5 orders of magnitude greater for neutron absorption in cadmium compared to carbon. Therefore in the 1 MeV equivalent calculation we assumed that neutrons below 0.2 eV are absorbed by the cadmium.

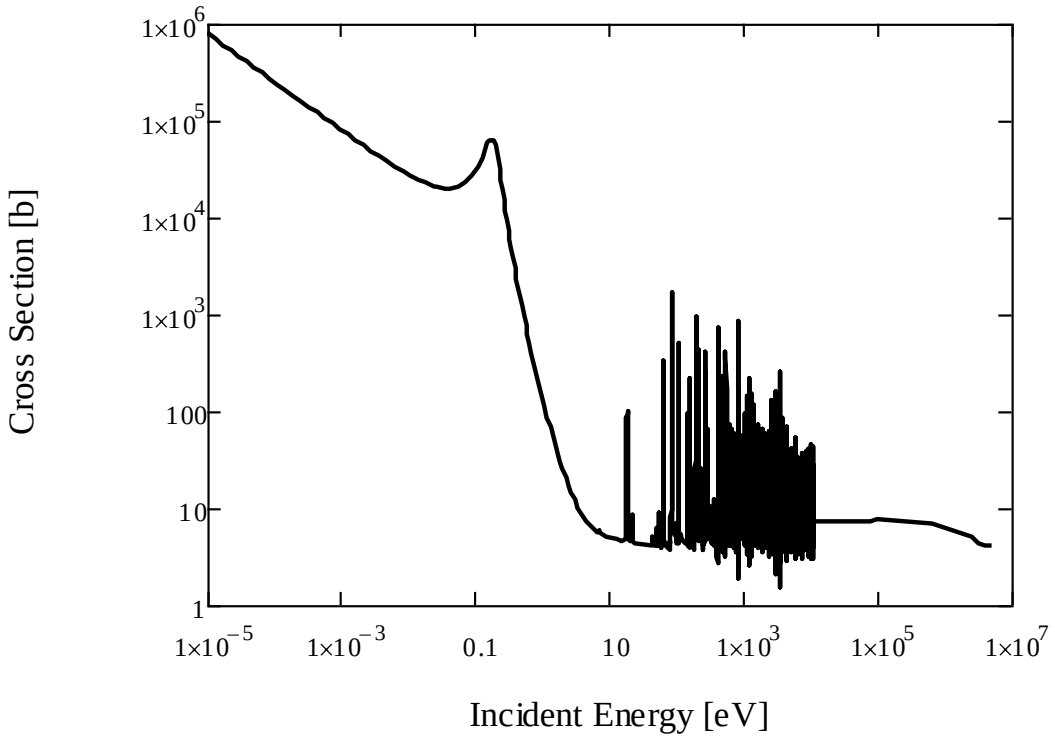

Figure 21. Cross section for Cadmium as a function of incident energy. [28]

The fluence level was determined by equating the NIEL effects of neutrons to electrons. A detailed explanation and calculations for equating the electron and neutron NIEL effects is found in Appendix A. As discussed in the electron irradiation section, the 35 year lifecycle for a satellite in space equates to a fluence of $1x10^{16} e^{-} / cm^{2}$. This value utilizes the electron flux value defined by MIL-STD 1809 as depicted in Table 1. The first step to find the neutron NIEL equivalent is to find the NIEL rate for electrons and neutrons. This was accomplished by figure 3.24 in [29]. An important note: the conversion factors were created for silicon. Obviously, applying this chart to our CNT and CNF composites introduces error in our calculation.

Using the conversion factor found in [29] led to the electron NIEL rate of $1.11x10^{-2}\ keVcm^2/g$ and a neutron NIEL rate of $1.10\ keVcm^2/g$. The second step is to use the NIEL rates above to find the expected amount of electron NIEL. This is accomplished by multiplying the NIEL rate by the electron fluence. This resulted in a NIEL of $1.23x10^{14}\ keV/g$. Thus, dividing the desired neutron and electron NIEL by the neutron NIEL rate will result in the desired neutron fluence. The fluence level of neutrons was determined to be $1.11x10^{14}\ neutrons/cm^2$. This value is the 1 MeV equivalent for neutrons due to the NIEL rates obtained in [29].

The third step in determining the time of irradiation in the rabbit tube was to convert the 1 MeV equivalent of neutrons into the spectrum of neutrons the OSURR produces. This conversion was accomplished using ASTM E722 [30]. Lastly, a neutron flux differential energy group was provided by the OSURR facility. Using ASTM E722 and the desired neutron fluence, it was calculated that the CNT and CNF samples would be irradiated for 9 minutes and 52 seconds in the rabbit tube.

Following the initial neutron irradiation, post irradiation resistivity and ESD measurements were taken. Following those measurements, a second neutron irradiation was conducted to fluencies of $1.25x10^{15}\ neutrons/cm^2$, $3x10^{15}\ neutrons/cm^2$, $4.25x10^{15}\ neutrons/cm^2$, and $4x10^{16}\ neutrons/cm^2$. One CNT and one CNF composite was irradiated to each of the above fluence levels. The first three samples were irradiated using the rabbit tube, while the last and highest fluence level was irradiated in the CIF. The CIF was needed in order to accomplish the high dose level. Table 6 summarizes the

second irradiations. Following the irradiations, resistivity measurements were taken on all samples.

Table 6. 1 MeV equivalent fluence levels of the second neutron irradiation and the time and locations of irradiations in order to achieve the associated fluence level. One CNT and one CNF composite sample was irradiated at each level.

1 MeV equivalent Fluence [neutrons/cm^2]	Location	Time [minutes]
1.25×10^{15}	Rabbit Tube	110
3×10^{15}	Rabbit Tube	276
4.25×10^{15}	Rabbit Tube	376
4×10^{16}	CIF	266

3.6 Thermal Cycling Measurements

In addition to the space radiation, the space thermal environment was simulated and the effects on resistivity were explored. The space thermal environment was simulated using a thermal cycle machine located at AFIT. The thermal cycle apparatus is shown in Figure 22. This cycled the samples from approximately -60 $^{\circ}$C to +60 $^{\circ}$C. The samples were held at each temperature for approximately 10 minutes before cycling to the opposite temperature. The number of cycles represented approximately a 10 year lifecycle of a satellite in space. This resulted in 4,963 cycles between -60 $^{\circ}$C and +60 $^{\circ}$C.

Figure 22. Picture of the thermal cycle apparatus used to simulate the space thermal environment.

The CNT, CNF, control and external configurations of the nickel nanostrand samples were all subjected to thermal cycling. Following thermal cycling, resistivity measurements were taken and compared to non-thermal cycled samples.

The nickel nanostrand samples used were of variable thickness. Due to the fabrication process, samples from different sheets had different thicknesses. When finding the volume resistivity, the different thicknesses between sheets resulted in inconsistent volume and surface resistivity measurement between sheets. Thus, trying to compare a non-thermal cycled sheet with a thermal cycled sheet was difficult due to the difference in thickness when using equation (2). A more accurate procedure to measure

thermal cycle effects would be to measure the resistivity on the same sample pre and post thermal cycle.

A possible solution would be to use equation (3) and find the surface resistivity. This measurement would remove the thickness from the calculations. However, this was attempted and similar results were found using surface resistivity and volume resistivity. It is believed the increase in thickness during the fabrication process changes both the surface and volume resistivity of the sample. The fabrication process needs to provide consistent material of equal thickness to compare the sheet resistivity.

IV. Results and Analysis

4.1 Overview

The CNT and CNF composites responded differently both pre and post irradiation. The CNT composites are more conductive than the CNF composites both pre and post irradiation. However, both electrons and neutrons, had a greater impact on the conductivity of the CNT composite. In addition, the changes in resistivity displayed by the CNT composite post electron irradiation, showed a room temperature annealing effect with time. The electron and neutron radiation had little impact on the CNF composite's conductivity.

4.2 Pre Irradiation Resistivity Results and Analysis

The CNT and CNF composites resistivity were measured prior to irradiation. Four samples of each type were used to determine the average volume resistivity for a sheet using equation (2). The samples were taken from the same sheet but were not cut adjacent to each other. The four sample measurements were averaged for the overall volume resistivity for the sample sheet. Table 7 shows the results of the four point resistivity measurements prior to any irradiations.

Table 7. Volume resistivity/conductivity measurements using equation (2) and equation (4) taken prior to any irradiations. The composites in rows 2 and 3 were used for neutron irradiations. The composites in rows 5 and 6 were used for electron irradiations.

	Resistivity [Ω-cm]	Conductivity [S/cm]
CNF Composite	0.16	5.8
CNT Composite	0.0094	106.8
CNF Composite	0.3496	2.9
CNT Composite	0.0091	109.9

The uncertainty in the CNF composite measurement was +/- 0.01 Ω-cm. The uncertainty in the CNT composite measurements was +/- 0.0003 Ω-cm (or 0.3 mΩ-cm . The CNT and CNF composites, had identical dimensions between the width, probe spacing, and thickness. Therefore, a comparison between the resistance would equal a comparison of the resistivity. Figure 23 shows the difference in resistance between the CNT and CNF composites. The difference in slope represents the difference in resistivity in Figure 23.

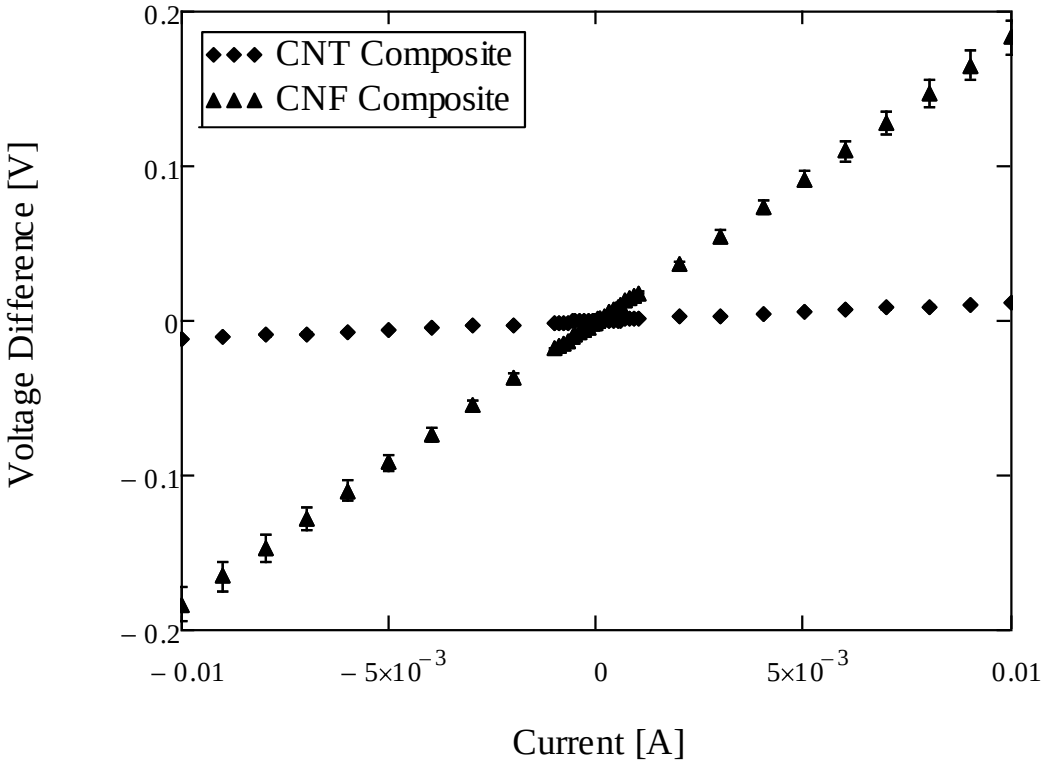

Figure 23. Four point probe measurement on the CNT and CNF composites. The difference in slopes represents the difference in resistance between the two composites.

When comparing both of the carbon samples to the nickel nanostrand samples, the CNT composites were slightly more conductive than the nickel nanostrand composites.

[1] reported a resistivity value of 0.020 Ω-cm for the nickel nanostrand samples. The CNF composite are more resistive then both the CNT and nickel nanostrand composites, however, the conductivity value according to ASTM B193 would still identify it as a conductive material. A value of 1 Ω-cm would be necessary for it to be considered a moderately conductive material according to ASTM D4496.

The large uncertainty associated with the measurement is a limitation to the measurement technique used with the composite material. Consecutive measurements using the four point probe test fixture without readjusting the sample resulted in small changes in resistance. However, when the sample was removed and then placed into the test fixture between measurements, a different resistance was found. This is indicative of the current taking a different path through the conductive layers nanoparticles when the probes were placed in a slightly different position. Therefore, we can conclude the nanofiller in both composite materials are not uniformly distributed throughout the epoxy.

Upon considering the three materials for protection against electrostatic discharge, all three materials provide enough conductive flow for charge to relax and not discharge across the internal components of a satellite. All composites are classified as a conductive material according to ASTM B193 and ASTM D4496. Prior to exposure to a radiation environment, the CNT composite material is the best material for a satellite structure with respect to its conductive properties.

4.3 Post Electron Irradiation Resistivity Analysis

Two electron irradiations were conducted on the CNT and CNF composite. The first electron irradiation, replicated the fluence level of both [1] and [2] consisting of $1\times10^{16} e^{-} / cm^{2}$. Table 8 shows the results of the post electron irradiation measurements and compares them to the pre-irradiation volume resistivity measurements.

Table 8. Volume resistivity/conductivity results post electron irradiation compared to pre irradiation resistivity/conductivity values. The fluence was $1\times10^{16} e^{-} / cm^{2}$. The percent change is shown in the last column.

	Resistivity [Ω-cm]	Conductivity [S/cm]	% Change
CNF Composite Pre Irradiation	0.3496	2.86	
CNF Composite Post Irradiation	0.3441	2.91	1.6
CNT Composite Pre Irradiation	0.0091	109.9	
CNT Composite Post Irradiation	0.0122	81.8	-25.5

The CNF samples had no change post electron irradiation. The change was 1% for the CNF samples. The post irradiation measurements had an uncertainty 0.001 Ω-cm. Therefore, a 1% change is within the uncertainty of the measurement. The CNT composite's resistivity did show a change post electron irradiation. The change was 25%. The uncertainty for post irradiation measurement was 0.4 mΩ-cm.

The CNT composite became more resistive while the CNF composite became slightly less resistive. These changes indicate the CNF composite resistivity will not be affected by the electron space radiation over the lifetime of a satellite. The CNT composite will be affected by the electron space radiation environment. However, due to

the different conductivity of each material prior to the irradiation, the CNT composite remains superior to the CNF composite.

The same epoxy resin was used in the CNF and CNT composites. Therefore, since no resistivity change was observed in the CNF composite and a change was observed in the CNT composite, we can conclude the change is occurring in the nanofiller particles and not in the epoxy. [1] postulated that the change in resistivity was the creation of free radicals within the epoxy resins. However, with no change in the CNF composite observed following electron irradiation, the change is most likely to occur within the nanoparticle.

The atomic displacements of the carbon atoms within the CNT's reduce the conductivity of each CNT [31]. The CNT composites consisted of SWNT and MWNT, the SWNT are more susceptible to radiation damage. This is because the SWNT only consists of a single atomic layer. When considering an atomic displacement on a SWNT, the displaced atom will bind together with an adjacent molecule of the epoxy resin, thus having a greater effect on the resistivity of the SWNT.

As has also been found with focused electron irradiation, the displacement damage causes deformation of the dimensions of the CNT's [31]. The deformation of the CNT's will cause a change in the electrical properties. This is because the conductivity of the CNT's are determined by the CNT diameter and chirality [32]. The deformation caused by the electron radiation would change the diameter of the CNT's.

However, when considering an atomic displacement of a MWNT, the displaced atom can bind together with an adjacent molecule of the epoxy resin or with an adjacent carbon atom from another layer of the MWNT. If it binds with another layer of the

MWNT it will have little effect on the resistivity of the MWNT. Electron spin Resonance (ESR) studies have found MWNT to be much more resistant to radiation damage due to the multi-wall nature of the CNT's compared to the SWNT [33].

The small change in the CNF composite can be explained similarly. The TEM images from section II show the stacked cup formation of the sheets of graphene. Therefore, displaced atoms have a high probability to bind with another carbon atom from an adjacent layer of graphene much like a MWNT.

The second electron irradiation provided a fluence of $6\times10^{16}e^{-}/cm^{2}$. As shown in Table 9, the CNF composite had little to no change from the pre irradiation resistivity measurements. The uncertainty in the post irradiation CNF measurement was +/- 0.4 mΩ-cm. This indicates the CNF composite conductivity will not be affected by an electron radiation environment much higher than what is experienced in space.

Table 9. Results of the second electron irradiation volume resistivity measurements with reported changes from pre irradiation measurements. The fluence was $6\times10^{16}e^{-}/cm^{2}$.

	Resistivity [Ω-cm]	Conductivity [S/cm]	% Change
CNF Composite Pre Irradiation	0.3496	2.86	
CNF Composite Post Irradiation	0.3524	2.84	-0.8
CNT Composite Pre Irradiation	0.0091	109.9	
CNT Composite Post Irradiation (3 days)	0.0112	89.5	-18.5
CNT Composite Post Irradiation (12 days)	0.0099	101.0	-8.1

The results of the second post electron irradiation for the CNT composite are also shown in Table 9. Two resistivity measurements of the CNT composite post irradiation. The first measurement was taken 3 days after the irradiation, the second measurement was taken 12 days after the irradiation. The measurements resulted in different values. The CNT composite was expected to be more resistive after the second and higher fluence irradiation than after the first and lower fluence irradiation. As shown in Table 9, the CNT composite became less resistive after exposure to the higher electron fluence after 3 days of room temperature anneal compared to only 2 hours after the first irradiation.

Due to the lower change in resistivity, another measurement was taken 12 days after the irradiation to explore the idea of an annealing process associated with the electron radiation. As shown in Table 9, the CNT composite became less resistive after 12 days. Therefore, the change in resistivity of the CNT composite post electron radiation anneals over time reducing the resistivity of the material.

The CNT composite annealed over the 12 days, however it did not recover back to the pre irradiation resistivity. An 8.1% change from the pre irradiation resistivity remained after the 12 days and remained constant for measurements conducted after 12 days. The resistivity measurement taken after the first and lower electron irradiation was taken 2 hours after the irradiation was completed.

Both ionizations and atomic displacements are initially reducing the resistivity. As discussed previous, the atomic displacement results in a carbon atom being displaced from its lattice position, which results in deformation of the CNT structure. A CNT has a hexagonal lattice structure. When atomic displacements occur, the hexagonal lattice

structure is broken with primary knock on atoms and interstitial atoms. The first mechanism to the room temperature (RT) anneal process is through dangling bond saturation and by forming non-hexagonal rings [31]. The second mechanism is through the migration of a carbon interstitial atom [31]. Figure 24 depicts the two anneal mechanisms.

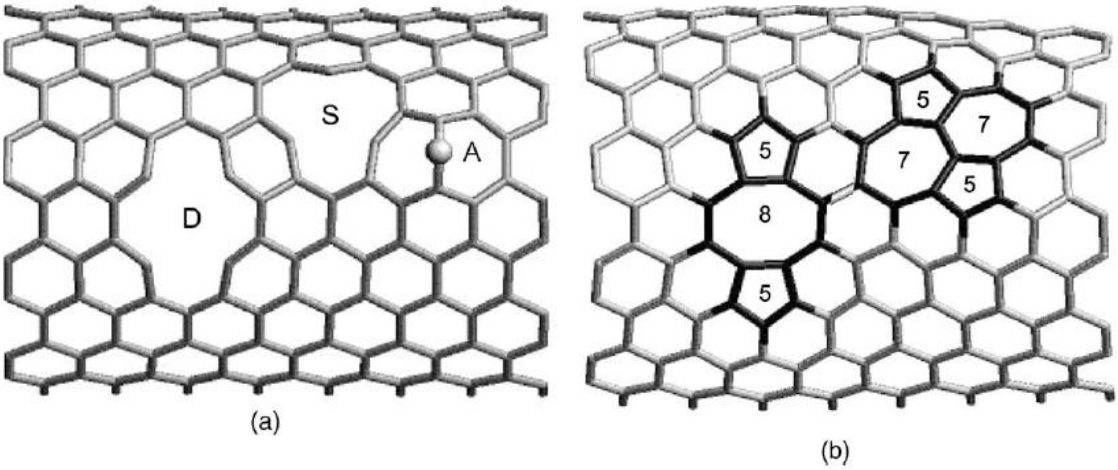

Figure 24. The two mechanisms that cause the CNT to anneal. (a) atomic displacements caused by electron radiation before anneal. D depicts two atomic displacements, S depicts one atomic displacement, A is an interstitial carbon atom. (b) The anneal process, D forms non-hexagonal rings, S anneals by the migration of the carbon interstitial atom [31].

The measurement taken after the first electron irradiation in Table 8 shows an increase in resistivity due to ionizations and atomic displacements. The measurement taken 3 days after electron irradiation in Table 9 shows an increase in resistivity due to ionizations and atomic displacements with some annealing. While the measurement taken 12 days after electron irradiation in Table 9 shows an increase in resistivity due to the two anneal mechanism discussed above. The annealing process also accounts for the

higher resistivity measurement taken after the first and lower fluence electron irradiation due to the measurement taken only 2 hours after irradiation.

4.4 Post Neutron Resistivity Analysis

Two neutron irradiations were conducted on the CNT and CNF composites. The first neutron irradiation, shown in Appendix A, was equivalent to the electron NIEL effects for a 35 year lifecycle of a satellite in geosynchronous orbit. Table 10 shows the results of the post neutron irradiation resistivity measurements.

Table 10. Volume resistivity/conductivity for pre and post neutron irradiation. The neutron fluence was $1.11\times10^{14}\ neutrons/cm^2$. The change in resistivity is shown in the last column.

	Resistivity [Ω-cm]	Conductivity [S/cm]	% Change
CNF Composite Pre Irradiation	0.1592	6.28	
CNF Composite Post Irradiation	0.1576	6.35	1.0
CNT Composite Pre Irradiation	0.0094	106.4	
CNT Composite Post Irradiation	0.0098	102.5	-3.7

The CNF composites change in resistivity by an average of 1% with an uncertainty in the post irradiation measurement of +/- 0.005 Ω-cm. The CNT composites increased resistivity by 3.7% with an uncertainty in the post irradiation measurement of +/- 0.2 mΩ-cm. The expected change in resistivity for this neutron irradiation was the same as the change in resistivity for the first electron irradiation.

Looking at the CNF samples, the change in resistivity post-electron irradiation was 1.6% while post-neutron irradiation the change was 1%. Looking solely at the CNF

composite, the neutron fluence level of $1.11\times10^{14}\,neutrons/cm^2$ accurately replicated the electron NIEL effects for a 35 year satellite lifecycle. However, the similarity in the change in resistivity may be due to the radiation hardness of the CNF composite and it would take a much higher dose to see a change in resistivity. The CNF "stacked cup" design is more resistant to atomic displacement damage that occurs when exposed to electron and neutron radiation. However, the drawback is the higher starting resistivity compared to both CNT and nickel nanostrand composites.

The CNT composite showed an increase in resistivity of 3.7% with an uncertainty in the post irradiation measurement of +/- 0.018 Ω-cm. This change does not replicate the changes that were observed for the first electron irradiation. An overall change of 25.5% in resistivity for the first electron irradiation was measured. However, as discussed before, the 25.5% increase was due to ionization and atomic displacement damage measured only 2 hours after irradiation. The measurement taken post neutron irradiation that resulted in a 3.7% change was taken 4 days after irradiation due to activation of the impurities in the composite. Therefore, any atomic displacement damage that occurred had sufficient time to anneal.

The second neutron irradiation involved irradiating the 4 CNF and 4 CNT samples to increasing fluence levels. Figure 25 shows the results for the 5 additional neutron fluence levels. One CNT and one CNF sample was irradiated at each neutron fluence level. In order to compensate for the variation in pre irradiation conductivity, the percent change from the individual sample was applied to the average pre neutron irradiation conductivity. As shown in Figure 25 and Table 11, the CNT composite conductivity continually decreases with increasing neutron fluence. The CNF composite

conductivity has little change up to a neutron fluence of $4\times10^{16} neutrons/cm^2$ 1 MeV equivalent. This neutron fluence equates to an electron fluence of $4\times10^{18} e^{-}/cm^2$.

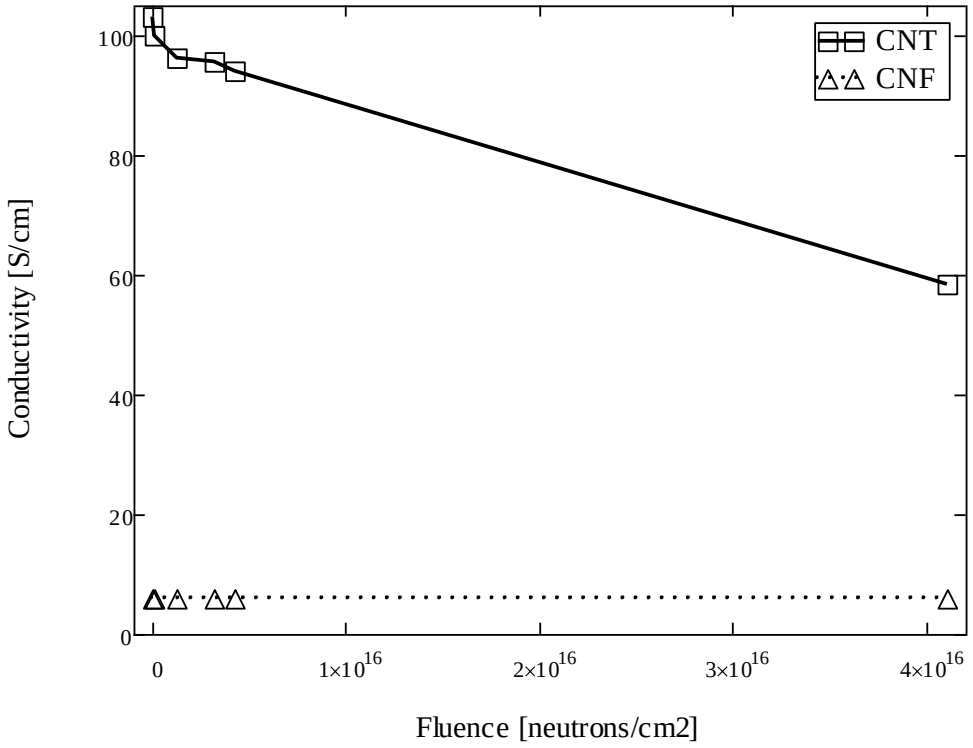

Figure 25. The reduction in volume conductivity as a function of neutron fluence in the CNT and CNF composite materials.

Table 11. Changes in volume resistivity/conductivity due to a corresponding neutron fluence for the CNT composite only. CNF composite resistivity remained constant.

1 MeV equivalent neutron Fluence [neutrons/cm^2]	Volume Conductivity [S/cm] CNT Composite	Volume Conductivity [S/cm] CNF Composite
0	103.1	5.8
1.11E+14	100.1	5.9
1.24E+15	96.3	6.0
3.11E+15	95.8	6.0
4.24E+15	93.9	5.9
4.10E+16	58.5	6.0

Due to the timing of the post electron irradiation measurements, no comparison could be made between the 35 year satellite lifecycle electron fluence and neutron fluence. However, we can equate the second electron fluence of $6\times10^{16} e^{-}/cm^{2}$ to a neutron fluence of $6\times10^{14} neutrons/cm^{2}$ using the same method described in section III and shown in Appendix A. Furthermore, we can use Figure 25 to find the expected neutron induced conductivity change. The interpolated conductivity change using Figure 25 results in a neutron induced change of 4.54%. We can now compare this to the electron induced conductivity change at the equivalent fluence of 8.1%. This provides for a much better comparison for the damage due to atomic displacements with RT annealing after both types of radiation.

4.5 Electrostatic Discharge Measurement Analysis

The ESD test designed by [1] introduced a measurement that attempted to find the ESD properties of a material as well as finding an alternative measure of the transverse or bulk resistivity. Obviously the ESD measurement is not a direct measurement of the bulk resistivity; however certain parameters of the current waveform from the ESD test can provide information of the bulk resistivity. The three specific parameters of interest will be I_{peak}, rise time and fall time of the early peak.

The I_{peak} amplitude is a measure of the overall resistivity of the material [1]. In addition, the rise and fall time of the first peak are also indicative of the resistivity of the material. The four point probe measurements gave us the surface and volume resistivity of the CNT and CNF epoxy layers. However, for the ESD test, the insulating S-glass makes up 90% of the material the ESD test is measuring. This is obstacle to getting

usable ESD results. Any changes in the output waveform are indicative of the S-glass and the conductive layer, whether the conductive layer is CNT's or CNF's. Therefore, a comparison of the CNT versus the CNF composites waveforms are made in order to account for the S-glass present in both composites.

Figure 26 shows the current waveforms of the CNT and CNF composites prior to any irradiations. We assume the resistivity of the S-glass in both composites is equal. Therefore, any difference in waveform would be due to the CNT or CNF layer. From the four point resistivity measurement, we know the CNF lateral resistivity is greater than that of the CNT. Therefore, we would expect the bulk resistivity to follow those results if the nanoparticles are spread uniformly in both the x and y cardinal direction. A deviation from the lateral resistivity would indicate non uniformities in the nanoparticle spread throughout the resin in all directions.

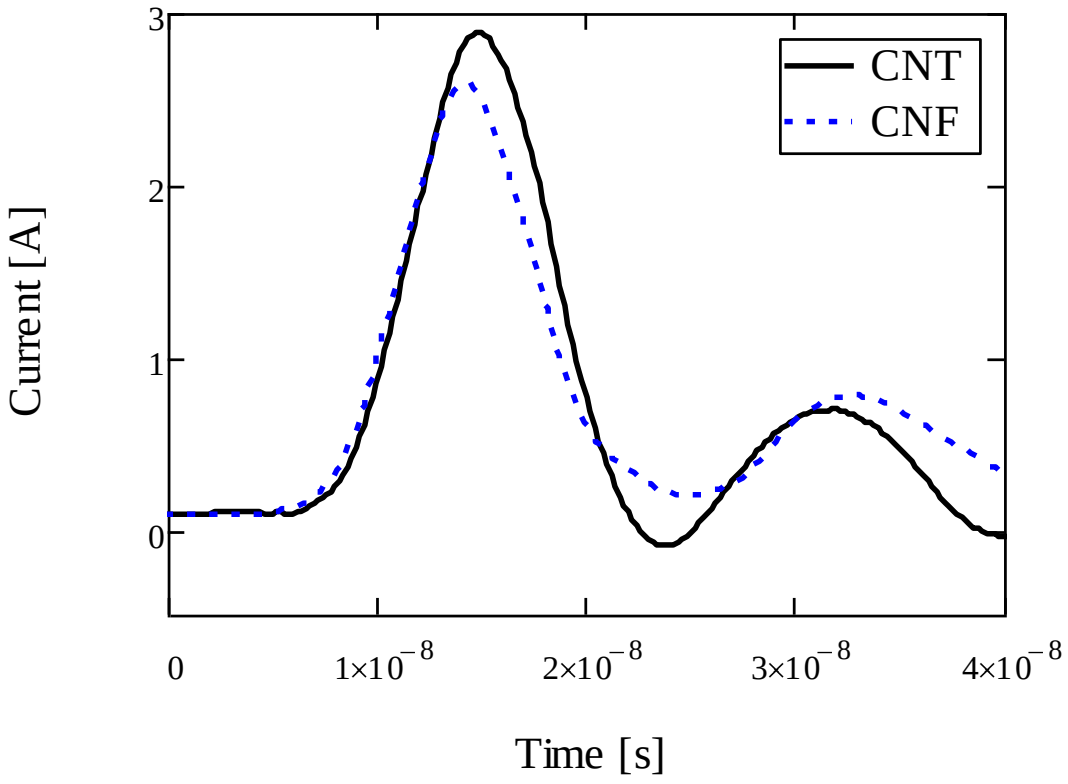

Figure 26. ESD waveforms of the CNT and CNF composite materials pre irradiation.

As shown in Figure 26, I_{peak} is different for the CNT and CNF composite. The CNT composite I_{peak} was 2.634 A, while the CNF composite was 2.341 A. This is indicative of a higher bulk resistivity in the CNF composite than the CNT composite. Additionally, the CNF composite is more susceptible to ESD. However, the rise and fall time of the early peak appear to be approximately the same. This is likely due to the insulating S-glass rather than the conductive layer. Next, an ESD measurement of the CNT composite pre and post neutron irradiation was made to explore a change in bulk resistivity due to neutron damage. The four point resistivity measurement indicated a decrease in lateral resistivity of the CNT composite. Therefore, we would expect a lower

I_{peak}. Figure 27, shows the ESD current waveform for the CNT composite pre and post neutron irradiation.

I_{peak} for post neutron irradiation for the CNT composite was 2.142 A as shown in Figure 27. The lower I_{peak} is indicative of an increase in bulk resistivity and an increased susceptibility to ESD. 2.142 A is lower than the pre neutron irradiation value for the CNF sample. This leads to the conclusion the bulk resistivity of the CNT composite is greater than the CNF composite prior to neutron irradiation. This is contradictory to the four point lateral resistivity measurements.

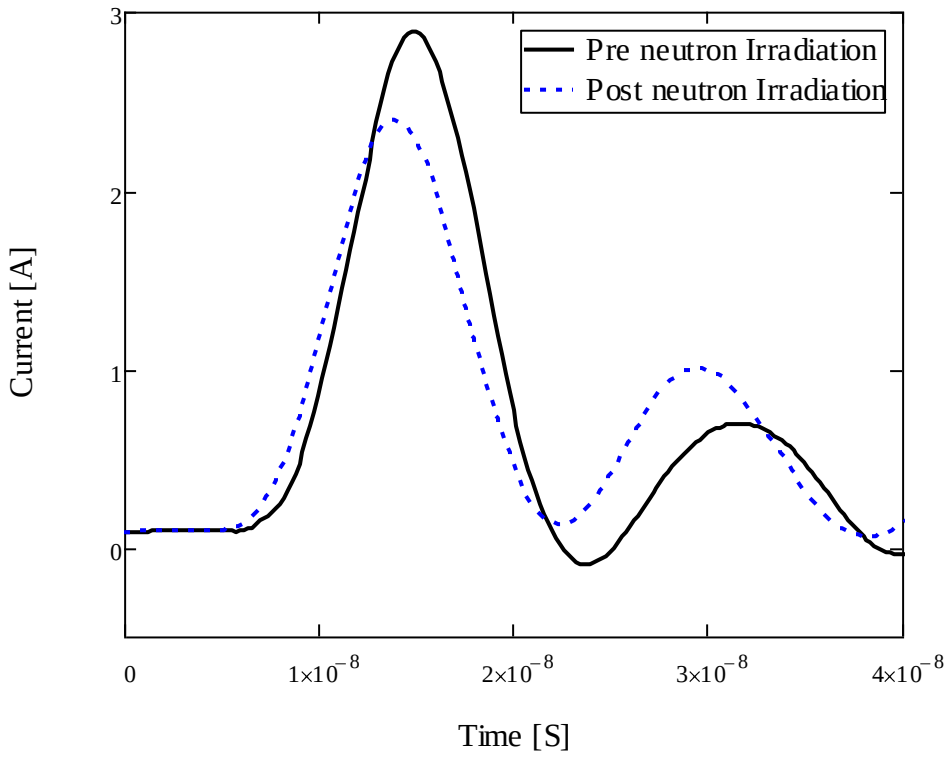

Figure 27. Smoothed ESD current waveform for the CNT composite pre and post neutron irradiation.

An ESD measurement of the CNF composite pre and post neutron irradiation was conducted to analyze the change in bulk resistivity. Figure 28 shows the results of the ESD measurement on the CNF composite. The four point lateral resistivity indicated no change in the resistivity of the CNF composite. Therefore, we would expect similar ESD waveforms pre and post irradiation.

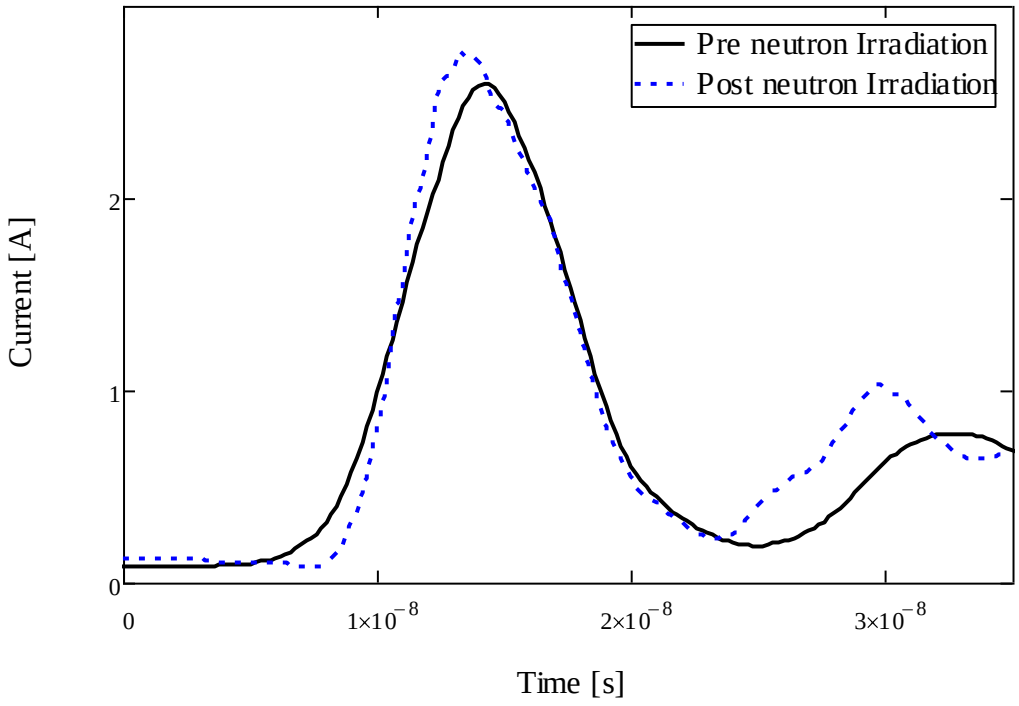

Figure 28. Smoothed ESD current waveform for the CNF composite pre and post neutron irradiation.

As shown in Figure 28, I_{peak} for the post neutron irradiation ESD measurement is 2.515 A which is higher than the pre irradiation I_{peak}. This increase in I_{peak} indicates a decrease in the bulk resistivity and decrease in the susceptibility to ESD.

Using the I_{peak} results from each measurement, one could conclude that the change in bulk resistivity is due to neutron radiation. There is a slight correlation between the four point lateral resistivity and the ESD measurement. However, the four point resistivity measurement takes the S-glass substrate completely out of the measurement and allows a measurement on the specific conductive surface layer. With the ESD measurement, the S-glass plays the primary role. This is most evident because the CNF and CNT conductive layer shows an order of magnitude difference in resistivity alone using the four point surface measurement, where the I_{peak} values in the ESD measurements were within 0.3 A. From the CASINO simulations, the majority of the radiation energy is deposited within the S-glass. The changes in S-glass were not an objective of this research.

Therefore, the four point resistivity measurement is a much better method for determining the changes in conductivity in the CNT and CNF composites due to radiation. This is because the measurement is able to isolate the CNT and CNF layer and ignore the S-glass substrate. If the S-glass substrate was removed from the composite, a better and more useful ESD measurement is possible. The ESD measurement designed by [1] was initially used on the nickel nanostrand composites which do not include any insulating material. The ESD measurement is suitable for conductive and semi-conductive material.

4.6 Post Thermal Cycle Resistivity Results

The results of the post thermal cycle resistivity measurements are shown in Table 12. Table 12 lists the surface and volume resistivity. As noted in section III, samples

were cut from different sheets for the pre and post thermal cycle measurements. The different sheets of the nickel nanostrand composites did not have a consistent thickness. The thickness of the composite resulting from inconsistent fabrication process affects the conductivity of the material. The thickness affects both the surface and volume resistivity. Therefore, the results in Table 12 for the nickel nanostrand composites are not a good representation of the changes due to thermal cycle.

Table 12. Volume and surface resistivity results of the composite materials pre and post thermal cycle.

	Volume Resistivity	Surface Resistivity	Conductivity
Sample	ρ [Ω-cm]	ρ [Ω/square]	σ [S/cm]
Control Pre Thermal cycle	0.009	0.103	105.4
Control Post Thermal cycle	0.009	0.059	107.2
% change	-1.7	-42.7	
EXT Pre Thermal Cycle	0.0085	0.047	117.3
EXT Post Thermal cycle	0.0092	0.049	109.0
% change	7.6	4.2	
CNT Pre Thermal Cycle	0.0094	0.94	106.7
CNT Post Thermal cycle	0.0110	1.10	90.7
% change	17.6	17.6	
CNF Pre Thermal Cycle	0.16	15.6	6.4
CNF Post Thermal cycle	0.35	34.8	2.9
% change	123.4	123.4	

However, SEM images of the CNF and CNT composites pre and post thermal cycle indicate no change in thickness was involved in the thermal cycle or in the fabrication process. Therefore, the comparisons in Table 12 are more accurate for the CNT and CNF composites. However, as discussed previously, different resistance

measurements were found on a single sample when the 4 probes were placed in slightly different locations. Even greater changes in resistance were discovered from sample to sample cut from different locations of a sheet or from different sheets altogether. This is due to non-uniformities in the nanofiller spread throughout the epoxy. Therefore, comparing one sample to another sample pre and post thermal cycling introduces error.

The CNT samples showed a decrease in resistivity by 17% and the CNF samples increased by 123%. Due to the discussion above, I believe the specific percent should be ignored, and only a comparison to one another should be made. Therefore, we conclude the thermal cycle had a larger impact on the CNF composite than the CNT composite.

The change in resistivity on the CNT and CNF composites can be explained by the thermal expansion and compression experienced by the nanofillers and the epoxy resin. During the cold cycle, the atomic structure of the material compresses. During the hot cycle, the atomic structure of the material expands. Thermal expansion is the growth of the material due to increasing the inter-atomic vibrations in the lattice of the material [35]. Conversely, thermal compression is due to decreasing of the inter-atomic vibrations of the material lattice.

The expansion and compression of the individual atomic elements that comprise the composite will be different due to the difference in atomic masses. Therefore, the CNT or CNF will expand and contract differently than the epoxy resin. As the nanofiller expands and contracts, the conductive pathway that was present will change during a thermal cycle. In addition, gaps can form from the expansion and compression of the composites and these gaps would increase the resistivity of the material due to a reduction in the conductive pathway once the material is brought back to RT.

IV. Conclusions and Recommendations

In conclusion, the CNT and CNF composites were irradiated with neutrons and electrons and changes to the lateral and transverse resistivity were explored. The lateral resistivity measurements, consisting of volume and surface resistivity using the four point probe measurement technique, are much more consistent and reliable than the ESD test developed to interpret changes in bulk resistivity. A lack of in-situ measurement using the four point probe technique is a limitation for this experiment. The time dependent RT anneal observed after the electron irradiation would have benefited from a measurement technique capable of measuring during and immediately following irradiation.

The CNT composite is the better material for protection against radiation when considering the conductive properties both prior to and following electron and neutron irradiation. The CNT is an order of magnitude more conductive than the CNF composite. However, the CNF composite is still a conductive material, and provides sufficient protection against ESD if used as a structural support of a satellite.

The simulated space radiation environment had little effect on both the CNT and CNF composite conductivity. The largest change in conductivity was 3.7% with the CNT composite following neutron irradiation. Less than 1.6% change was observed in the CNF composite. The 25.5% change observed post electron irradiation is believed to be effected by the time the measurement was taken. A lower percent change would have been measured if the measurement was taken after RT annealing was allowed to occur. Both composite materials are electrically hardened for the space radiation environment.

When the fluence of radiation was increased on the composites, the CNF conductivity remained constant while the CNT composite's conductivity decreased. The

most damaging radiation fluence was the neutron fluence of . The conductivity had no change in the CNF composite. However, the CNT composite changed by 43% at the highest neutron fluence.

The neutron radiation is the more damaging radiation compared to electron radiation on the composite materials. However, the neutron spectrum of the OSURR was converted to a 1 MeV equivalent. If only 1 MeV neutrons were incident upon the material, no conversion would be necessary and it would make for a better comparison. Only 0.5 MeV electrons were used and a majority of the electrons passed through the material causing less damage. No RT anneal was observed post neutron irradiation due to neutron activation of the materials and the inability to perform measurements. A test method that allows for in situ measurements would allow for an investigation into the anneal post neutron irradiation. This would allow for the discovery of the type of defects each radiation may produce.

Both CNF and CNT composites make for a good replacement for aluminum for satellite structures when considering their conductive properties and ability to withstand the radiation environment. However, due to the anneal effect that was discovered during the electron irradiation, further investigation should be explored into the prompt conductivity changes opposed to permanent changes. The earliest measurement taken for this investigation was two hours post irradiation. A measurement taken in-situ or within seconds post irradiation would lead to a better understanding of the radiation effects on the conductivity of the composites.

[1] postulated the changes in resistivity on the nickel nanostrand samples were due to the chemical changes in the epoxy. However, through this investigation, changes

in resistivity were due to changes in the nanoparticle. This is evidence by the change in resistivity in the CNT composite and no change in the CNF composite with the same epoxy in both. However, the epoxy used in the CNT and CNF composites is different than the epoxy used in the nickel nanostrand samples tested by [1] and [2]. A more direct measurement should be made on all three nanofillers using the same type of epoxy resin to ensure the changes observed by [1] and [2] were due to the epoxy.

Appendix A Equating the Electron and Neutron NIEL Effects

This appendix will show the steps that were taken to equate the electron and neutron NIEL effects. This allowed for a comparison of atomic displacements caused by different radiation types. The first step was to identify the electron flux in the space radiation environment. According to the table below that was created from MIL-STD-1809, the electron flux above 0.5 keV is equal to approximately $1\times10^{7} e^{-}/cm^{2}s$.

Table 13. Flux values defined by MIL-STD-1809

Source	Energy Range [MeV]	Flux [particles/cm^2-sec]
Protons	> 0.1	1×10^{7}
	> 1.0	1×10^{3}
Electrons	**> 0.1**	**2×10^{7}**
	> 0.5	**8×10^{6}**
	> 1.0	**2×10^{6}**
	> 2.0	**2×10^{4}**

The electron flux is converted into a fluence by multiplying by the lifetime of a satellite in space of 35 years. The total electron fluence is equal to $1\times10^{16} e^{-}/cm^{2}$. Step number two is to use figure 3.24 from [29] depicted below. Figure 3.24 gives the NIEL rate for electrons and for neutrons. 1 MeV was used as the particle energy. The NIEL rate for electrons is $1.1102\times10^{-2} kev-cm^{2}/g$. The NIEL rate for neutrons is $1.10\ kev-cm^{2}/g$. Figure 3.24 from [29] was created for Silicon. This introduces error when applying it to the composite materials. However, only an estimate was desired for the irradiations.

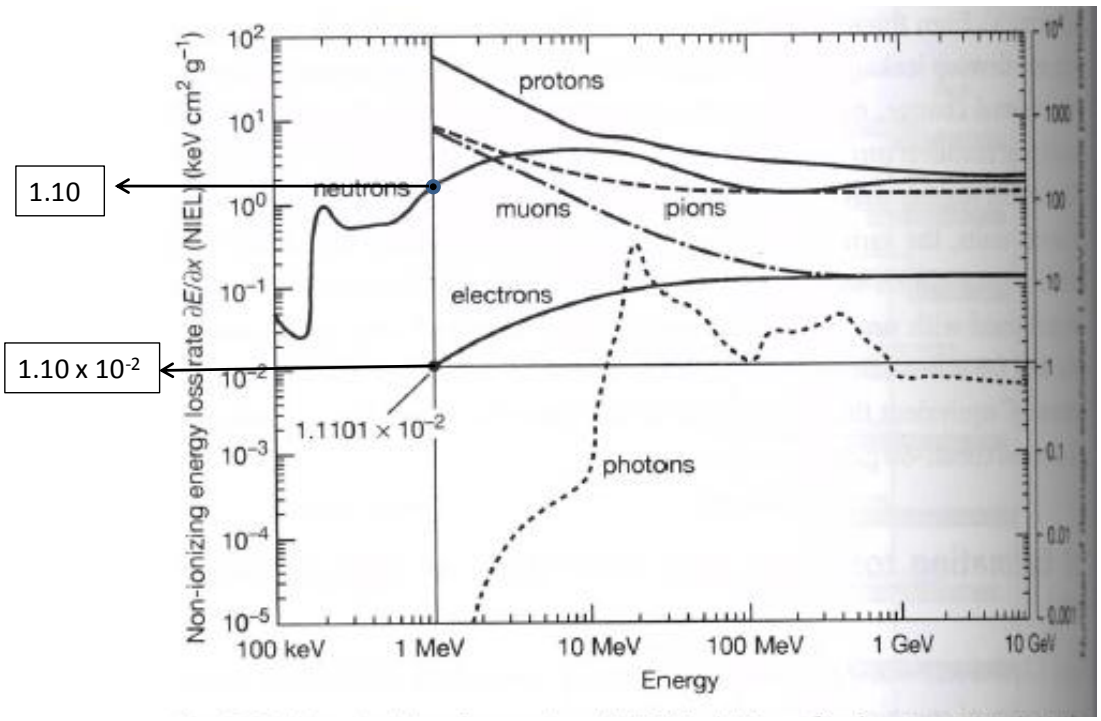

Figure 29. Figure 3.24 from [29]. The conversion factors are depicted.

The third step is to find the total amount of NIEL the > 0.5 MeV electrons will cause in the composite. Multiplying the NIEL rate by the electron fluence will give the overall NIEL in keV / g. Therefore, the electron NIEL is $1.23 \times 10^{14} keV / g$. Next, set the neutron NIEL equivalent to the electron NIEL. Using the neutron NIEL rate, find the 1 MeV neutron fluence by dividing the NIEL by the neutron NIEL rate. The neutron fluence equals $1.11 \times 10^{14} neutrons / cm^2$.

The OSURR does not produce monoenergetic neutrons at the rabbit tube beam port. Due to moderation of the water surrounding the core, a spectrum of neutrons is produced. Figure 30 below shows the differential neutron flux versus neutron energy in the rabbit tube beam port.

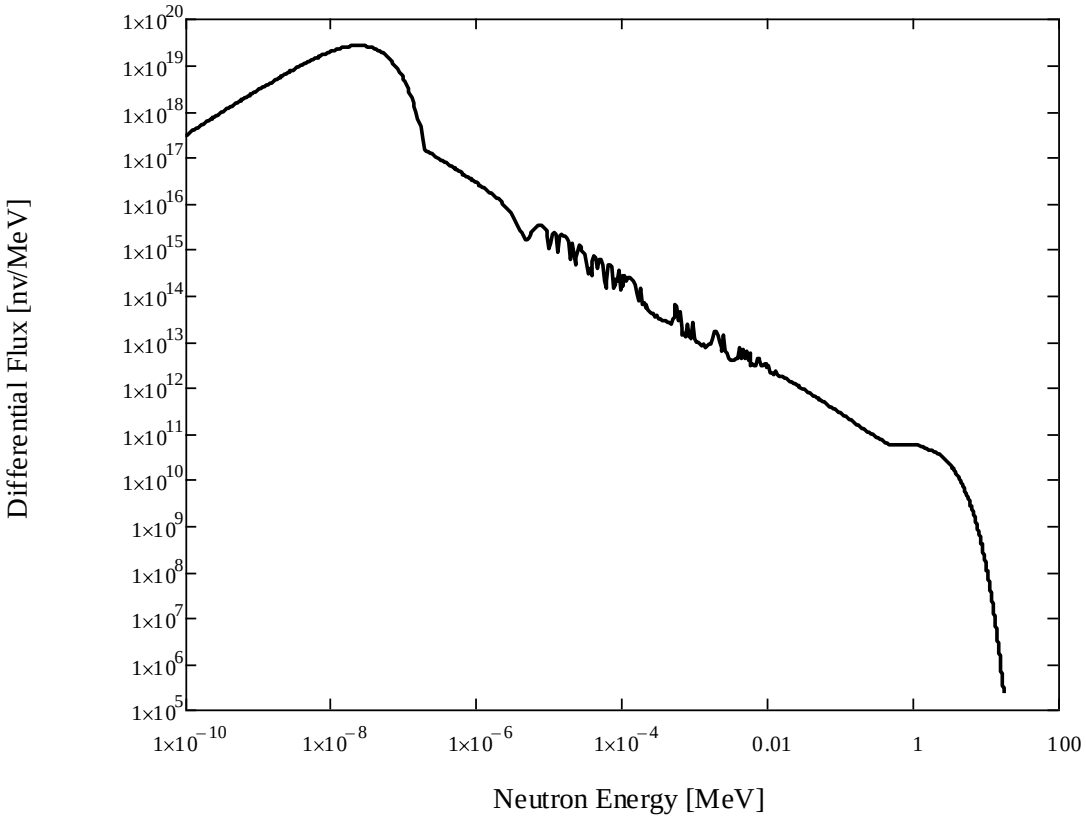

Figure 30. Neutron energy spectrum of the OSURR. [34]

ASTM E722-94 is the standard practice for characterizing neutron energy fluence spectra in terms of equivalent monoenergetic neutron fluence. Each composite sample was covered in cadmium in order to shield it from thermal neutrons. Cadmium has a high cross section for absorption for thermal neutrons. Neutron energies below 0.45 eV were assumed to be absorbed by the Cadmium and not included in the neutron fluence. The 1 MeV equivalent monoenergetic neutron fluence, $\Phi_{eq,1MeV,Si}$ is found using equation (6).

$$\Phi_{eq,1MeV,Si} = \frac{\int_0^\infty \Phi(E) F_{D,Si}(E) dE}{F_{D,1MeV,Si}} \qquad (6)$$

Where $\Phi(E)$ is the incident neutron energy-fluence spectral distribution, $F_{D,Si}$ is the neutron displacement damage function for Silicon as a function of energy, and $F_{D,1MeV,Si}$ is the displacement damage reference value designated for Silicon for 1 MeV. For the conversion for the rabbit tube beam port, E_{min} was set at 0.5 eV and E_{max} was set at 1.8 MeV in place of 0 and ∞ in the integral in equation (6). $F_{D,Si}$ for each energy is found in table A1.1 of ASTM E722. The values in table A1.1 were multiplied by 3.45×10^{-13} to convert to rad(Si)-cm^2. $F_{D,1MeV,Si}$ is given in ASTM E722 as 95 MeV-mb. Simpsons rule was used to carry out the integral in equation(6). The resulting 1 MeV equivalent neutron flux in the rabbit tube beam port is equal to $1.88\times10^{11} neutrons/cm^2 s$. Using the desired neutron fluence and the neutron flux the total amount of time of irradiation was determined to be 9 minutes and 52 seconds.

The same 1 MeV equivalent conversion was made for the differential flux spectrum for the CIF at the OSURR. The resulting 1 MeV equivalent neutron flux in the CIF is $2.57\times10^{12} neutrons/cm^2 s$. This higher flux allowed for a much higher neutron fluence. Figure 31 is a flow diagram that summarizes the conversion and uses the results of each step described above to find the time of neutron irradiation.

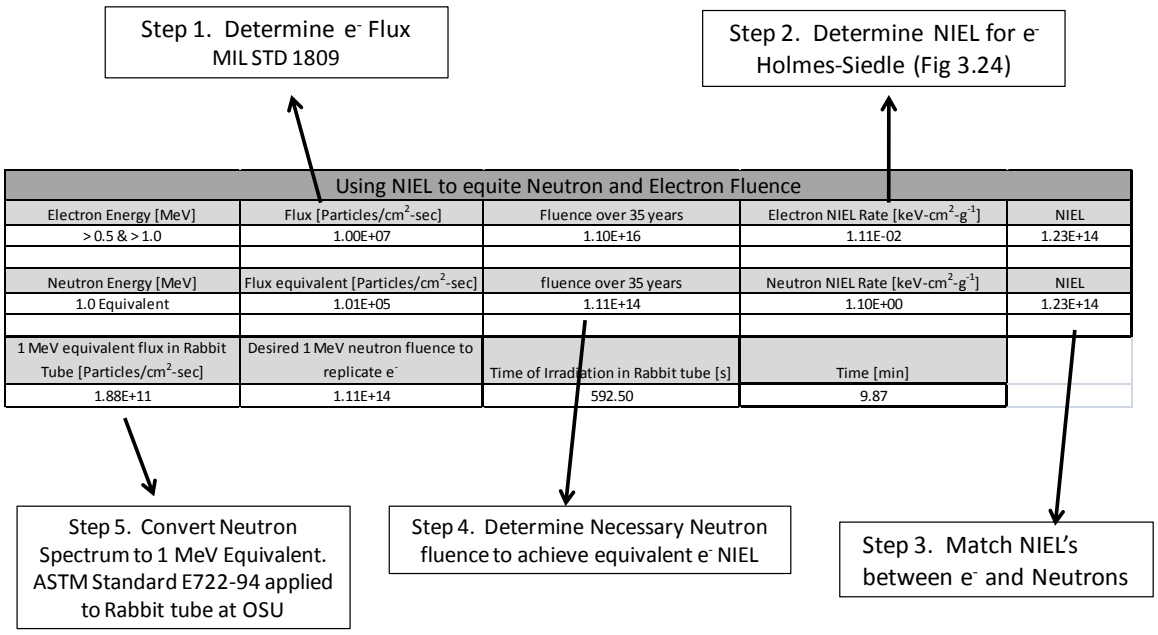

Figure 31. Flow diagram for equating the electron and neutron NIEL effects in Silicon and then converting the neutron energy fluence spectra into a 1MeV equivalent.

Appendix B Example of Smoothing Routine on the ESD Current Waveform

The ESD test output current waveform from the oscilloscope is depicted in Figure 32. The waveform is very noisy and does not follow the ideal waveform from [24] depicted in Figure 16. [1] conducts a detailed discussion of the intended output. However, due to the S-glass substrate and overall composite samples and associated test set-up, a noisy waveform is expected as shown in Figure 32.

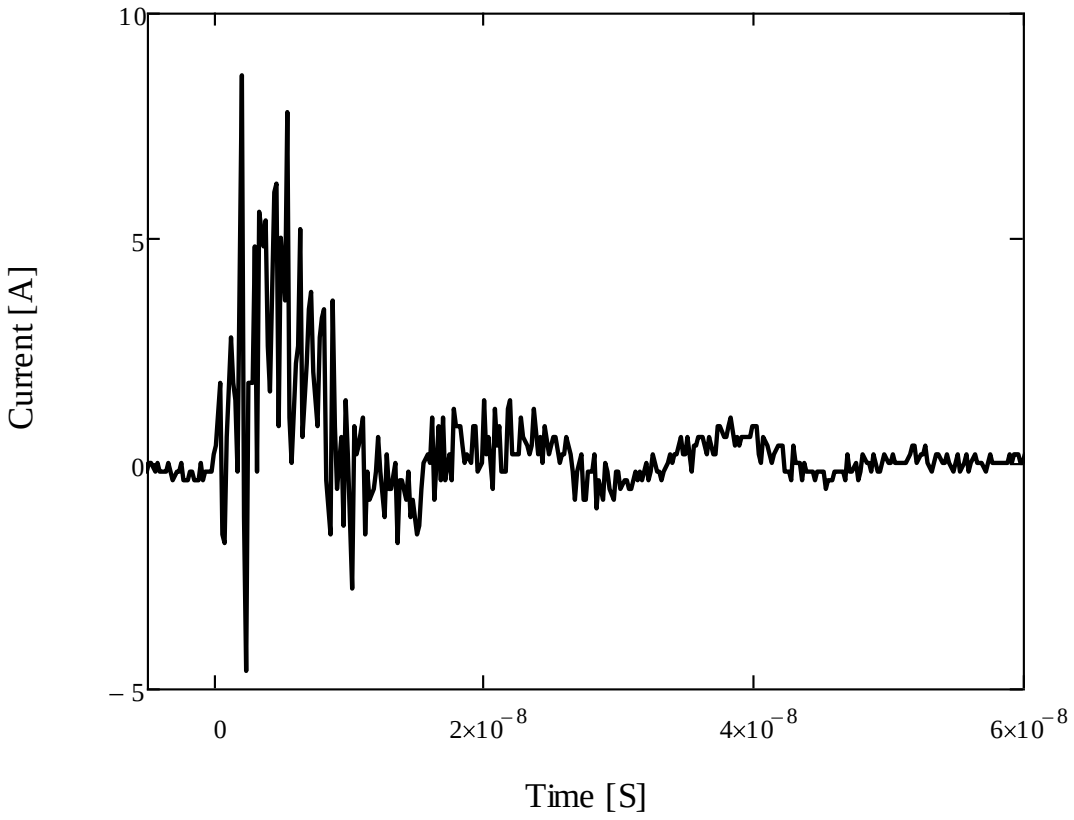

Figure 32. ESD current output from the oscilloscope.

A smoothing algorithm was used to smooth the current waveform. This allowed for a better view and overall trends of the waveform. It also would keep key features such as the early and late peaks for analysis, while throwing out the noise. A localized

linear fit line was used to smooth the data as shown in Figure 33. The resulting smoothed data is easier to analyze.

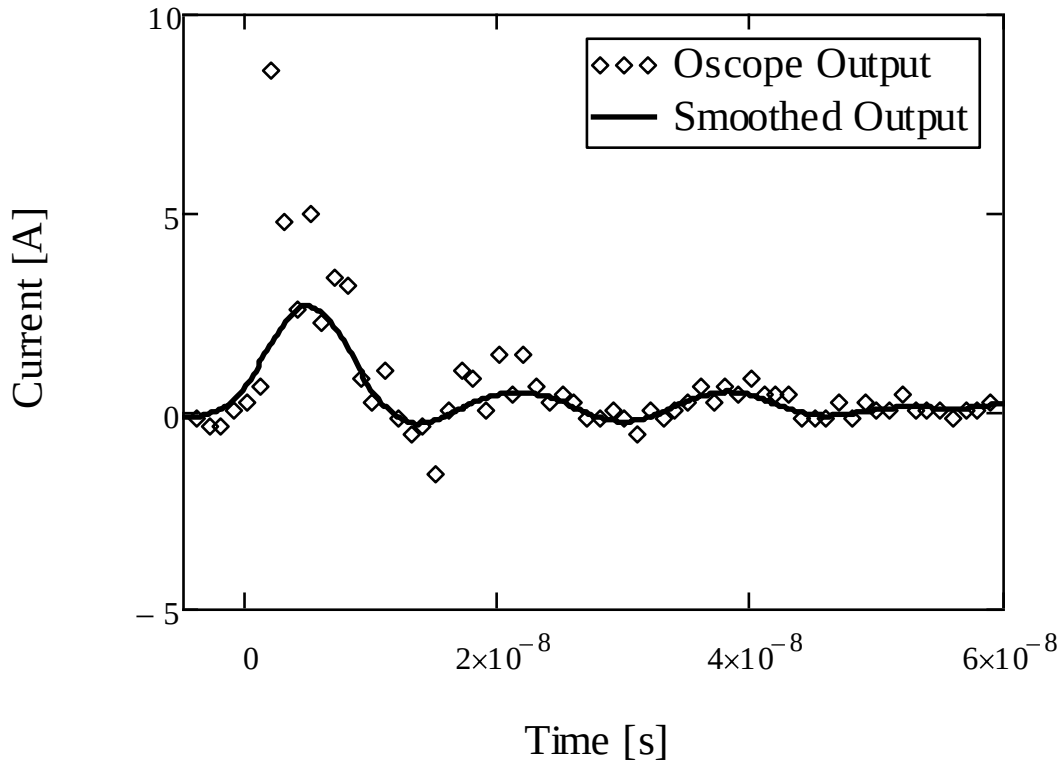

Figure 33. The original ESD output is plotted with the smoothed data. A localized linear fit is used to create the smoothed data.

Bibliography

[1] McGary, Joshua, D. *Electrostatic Discharge Properties of Irradiated Nanocomposites*. MS Thesis, AFIT/GNE/ENP/09-M03, Department of Engineering Physics, Air Force Institute of Technology (AU), Wright-Patterson AFB OH, 2009.

[2] Coy, David, F. *Changes To Electrical Conductivity in Irradiated Carbon-Nickel Nanocomposites*. MS Thesis, AFIT/GNE/ENP/10M-02, Air Force Institute of Technology(AU), Wright-Patterson AFB OH, 2010.

[3] R.H. Baughman, A.A. Zakhidov, W.A. de Heer. "Carbon Nanotubes-the Route Toward Applications," *Science*, 297, 787 (2002).

[4] Hansen, George. "High Aspect Ratio Sub-Micron and Nano-scale Metal Filaments," *SAMPE Journal*, 41(2), pp. 2-11, Mar. 2005.

[5] A.K. Geim. and K.S. Novoselov. "The Rise of Graphene," Unpublished Report. Manchester Centre for Mesoscience and Nanotechnology, University of Manchester, United Kingdom.

[6] Mall, Shankar. "Carbon NanoFiber produced at Applied Sciences." Electronic Message. 15 November 2010.

[7] NASA website http://imagine.gsfc.nasa.gov/docs/ask_astro/answers/970408d.html

[8] T. Berger "The Space Radiation Environment," website http://www.ati.ac.at/~vanwaweb/spacerad.html

[9] J. Catani, J. and D. Payan, "Electrostatic Behavior of Materials in a Charging Space Environment, in *2004* International Conference on Solid Dielectrics, 5-9 July, 2004, Toulouse, France.

[10] MIL-STD-1809, United States Air Force, "Space Environment for USAF Space Vehicles," February 15, 1991, pp. 20-23.

[11] E. S. Berman, J.A. Johnson, R.A. Mantz, P.S. Meltzer. "Spacecraft Materials Development Programs for Thermal Control Coatings and Space Environmental Testing." *AMPTIAC journal* Vol 8, Number 1, 2004.

[12] C. Gau, C.Y. Kuo, H.S. Ko. "Electron tunneling in carbon nanotube composites," *Nanotechnology journal*. Volume 20, Number 39: 3-7 (September 2009).

[13] Mall, Shankar and Petrosky, James. "Research Proposal for AS&T Outreach Program," Unpublished, pp 6, July 2010.

[14] Petrosky, James. Class handout, NENG 660, "Radiation Effects on Electronic Devices," Department of Engineering Physics, Air Force Institute of Technology, Wright-Patterson AFB OH, Summer 2010.

[15] Holmes-Siedle, Andrew. and Adams, Len. *Handbook of Radiation Effects*, New York: Oxford University Press, 2002.

[16] F. Banhart. "Irradiation of carbon nanotubes with a focused electron beam in the electron microscope." *Journal of Materials Science.* Vol 41 Number 14 July 2006.

[17] Sze, S.M. *Semiconductor Devices, Physics and Technology, 2nd Edition.* John Wiley & Sons, 2002.

[18] Shroder Dieter. *Semiconductor Material and Device Characterization*. New York: John Wiley and Sons, 2006.

[19] M.C. Evora. *Effect of Electron Beam Radiation On The Surface and Bulk Morphology of Carbon Nanofibers*. PHD Dissertation, School of Engineering, Unviversity of Dayton. May 2010.

[20] Tupta, Mary, A. "Techniques for Measuring the Electrical Resistivity of Bulk Materials." Keithley Instruments, Inc. Lecture given over Internet. 2010

[21] ASTM B193-02, "Standard Test Method for Resistivity of Electrical Conductor Materials," ASTM International, 2002.

[22] ASTM D4496-04, "Standard Test Method for D-C Resistance or Conductance of Moderately Conductive Materials," ASTM International, 2004.

[23] ASTM D257-07, "Standard Test Methods for DC Resistance or Conductance of Insulating Materials," ASTM International, 2007.

[24] P. Kodali, *Engineering Electromagnetic Compatibility*. New York: IEEE Press, 2001.

[25] MIL-STD-1541(A), United States Air Force, "Electromagnetic Compatibility Requirements for Space Systems," December 30, 1987.

[26] The Ohio State University Research Reactor website http://reactor.osu.edu/facilities/research-reactor

[27] The Ohio State University Research Reactor website http://reactor.osu.edu/pictures

[28] The National Nuclear Data Center website http://www.nndc.bnl.gov/sigma/getPlot.jsp?evalid=4365&mf=3&mt=1&nsub=10

[29] Holmes-Siedle, Andrew. and Adams, Len. *Handbook of Radiation Effects*, New York: Oxford University Press, 2002.

[30] ASTM E722-94, "Standard Practive for Characterizing Neutron Energy Fluence Spectra in Terms of an Equivalent Monoenergitic Neutron Fluence for Radiation-Hardness Testing of Electronics," ASTM international, 1994.

[31] Krasheninnokov, A V. and Nordlund, K. "Irradiation effects in carbon nanotubes." *Nuclear Instruments and Methods in Physics Research SectionB: Beam Interactions with Materials and Atoms.* 2004.

[32] Minot, Ethan. D, *Tuning the Band Structure of Carbon Nanotubes*, PHD Dissertation, Cornell University, August 2004.

[33] Beuneu, F, C. l'Huillier, J.P. Salvetat, J.M.Bonard, and L. Forro. "Modification of multiwall carbon nanotubes by electron irradiation: An ESR study," *Physical Review*, Volume 59, Number 8, February 1999.

[34] Talnagi, Joseph W. "Rabbit 450 KW May 2010." Electronic message with excel spreadsheet attachment.

[35] McKelvey, John, P. *Solid State Physics For Engineering and Materials Science*, Malabar: Krieger Publishing Company, 2003.

REPORT DOCUMENTATION PAGE

Form Approved
OMB No. 074-0188

1. REPORT DATE *(DD-MM-YYYY)*	2. REPORT TYPE	3. DATES COVERED *(From – To)*
24-03-2011	Master's Thesis	July 2010 – March 2011

4. TITLE AND SUBTITLE

Changes to Electrical Conductivity of Irradiated Carbon Nanocomposites

5a. CONTRACT NUMBER

5b. GRANT NUMBER

5c. PROGRAM ELEMENT NUMBER

6. AUTHOR(S)

Duncan, Nickolas, A., Captain, USA

5d. PROJECT NUMBER

5e. TASK NUMBER

5f. WORK UNIT NUMBER

7. PERFORMING ORGANIZATION NAMES(S) AND ADDRESS(S)

Air Force Institute of Technology
Graduate School of Engineering and Management (AFIT/EN)
2950 Hobson Way, Building 640
WPAFB OH 45433-8865

8. PERFORMING ORGANIZATION REPORT NUMBER

AFIT/GNE/ENP/11-M06

9. SPONSORING/MONITORING AGENCY NAME(S) AND ADDRESS(ES)

Defense Threat Reduction Agency
COL Mark Mattox
1900 Wyoming Blvd SE
Kirtland AFB, NM 87117-5669

10. SPONSOR/MONITOR'S ACRONYM(S)

DTRA/OP-CSU

11. SPONSOR/MONITOR'S REPORT NUMBER(S)

12. DISTRIBUTION/AVAILABILITY STATEMENT

APPROVED FOR PUBLIC RELEASE; DISTRIBUTION UNLIMITED.

13. SUPPLEMENTARY NOTES

14. ABSTRACT

Carbon nanotubes (CNT) and carbon nanofibers (CNF) are two nanoparticles incorporated in a polymer to create a composite material. These composites are two potential lightweight materials for use as replacements for aluminum structures on satellite systems. Both composite materials have a low resistivity that is consistent with conductive materials. However, the CNT composite is substantially more conductive than the CNF composite. The CNT and CNF composites were irradiated with electrons and neutrons to fluence levels of and . No changes were observed in the resistivity of the CNF composites following neutron and electron irradiation. A 3.7% increase in resistivity was observed for the CNT composite following neutron irradiation and a 25.5% increase in resistivity following electron irradiation. An additional electron irradiation was conducted on both composites to a fluence of . Again, no change in resistivity was observed in the CNF composites, while an 8.1% increase in resistivity was observed in the CNT composite. In addition, the CNT composite resistivity recovered after 240 hours while at room temperature. An additional neutron irradiation was conducted on both composites to a fluence to 4 . No change in the resistivity was observed in the CNF composite, while a steady increase in resistivity was observed in the CNT composites as a function of neutron dose.

15. SUBJECT TERMS

Conductive composites, radiation effects

79

16. SECURITY CLASSIFICATION OF:			17. LIMITATION OF ABSTRACT	18. NUMBER OF PAGES	19a. NAME OF RESPONSIBLE PERSON
a. REPORT	b. ABSTRACT	c. THIS PAGE			LTC John. McClory AFIT/ENP
U	U	U	UU	91	19b. TELEPHONE NUMBER *(Include area code)* (937) 255-6565, ext 7308 (emailname@afit.edu)

Standard Form 298 (Rev. 8-98)
Prescribed by ANSI Std. Z39-18